行政院國家科學委員會專題研究計畫　成果報告

利用高壓合成新材料及其特性分析(3/3)(中波國合計畫)

計畫類別：個別型計畫
計畫編號：NSC93-2113-M-002-001-
執行期間：93 年 02 月 01 日至 94 年 01 月 31 日
執行單位：國立臺灣大學化學系暨研究所

計畫主持人：劉如熹
共同主持人：楊弘敦
計畫參與人員：Subramanian Mylswamy, 王健源, 康佳正

報告類型：完整報告
報告附件：國際合作計畫研究心得報告
處理方式：本計畫可公開查詢

中　華　民　國 94 年 1 月 26 日

摘要**(Abstract)**

中文摘要

本計畫經由波蘭科學院之協助已設置完成高壓合成設備(壓力可達 1.5 GPa)，其包含三種不同之高壓反應裝置，並可於大範圍之壓力與溫度環境下合成樣品。

本計畫並建立以真空電弧鎔鍊爐於氬氣環境反應合成 YMn_2 合金，並於 800ºC 之真空狀態煆燒十一天以使其成分均勻。再以此 YMn_2 合金為起始物，於 200ºC 之高壓氘氣(1.7KPa) 之環境合成新型之氘化物 YMn_2D_6 合金，並以 X 光粉末繞射 (XRD)、中子繞射 (NPD)、高解析穿透式電子顯微鏡 (HRTEM)、X 光吸收近邊緣結構(XANES)與超導量子干涉(SQUID)分析 YMn_2D_6 合金之特性。

關鍵字

氘化物，高壓合成設備，真空電弧熔鍊，YMn_2 合金，YMn_2D_6 合金

英文摘要

High pressure piston-cylinder apparatus for pressure upto 1.5 GPa was designed and installed in our laboratory with the help of Polish Academy of Sciences, Poland. It consists of three different types of high pressure reactors which can be operated under different temperature and pressure conditions from low pressure/temperature combinations to high pressure/temperature combinations.

The YMn_2 intermetallic alloy was synthesized in an arc-melting chamber under argon atmosphere and annealed at 800ºC for 11 days in vacuum furnace to get homogeneity. The novel intermetallic deuteride YMn_2D_6 was synthesized at 200ºC under high deuterium pressure of 1.7 KPa. The material was characterized by advanced instrumental techniques such as X-ray diffraction (XRD), neutron powder diffraction (NPD), high-resolution transmission electron microscopy (HRTEM), Mn X-ray absorption near edge structure (XANES) and magnetization measurement (SQUID).

From the results of the above analysis crystal structure, valence state of Mn and magnetic properties were discussed in detail. Structure of YMn_2D_6 differs greatly from the parent C15 symmetry of the parent material which is unique property of this material.

keyword
Deuteride, High pressure apparatus, Arc-melting method, YMn_2 alloy, and YMn_2D_6 alloy

目錄

簡介 (Introduction)

Treatment of metals and alloys under high hydrogen/deuterium pressure proved to be an efficient synthetic technique to synthesize novel hydrides and deutrides. It has been used to synthesize many important hydrides of industrial importance such as NiH, MnH_x, FeH_x (1-3). In most of the cases the hydrides formed at high hydrogen pressure are not stable at normal conditions. It is expected that the application of high hydrogen pressure on intermetallic compounds may be extended to the hydrogen absorption to higher values with formation of new crystalline structures which are stable normal conditions.

In the present study we concentrate on the synthesis of YMn_2D_6 Laves phase deutride which is an interesting material among metal deutrides. The parent compound YMn_2 has unusual properties among intermetallic compounds. Under ambient conditions (4) this intermetallic Laves compound has a cubic C15 crystal structure with Fd-3m space group. The results of heat capacity and thermal expansion measurements as a function of temperature indicate that this compound exhibits a first order phase transition at T_N accompanied with a giant volume change of about 5%, which is ascribed to the spontaneous volume magnetostriction due to the collapse of the Mn moment at TN (5,6).

Another anomalous behavior of YMn_2 is its large thermal expansion coefficient above T_N. Such behavior can be interpreted by a rapid recovery of the amplitude of spin fluctuations with increasing temperature above T_N (7). Oomi et al. (8) found that the magnetism of YMn_2 is very sensitive to external pressure: the onset of magnetic order is not observable at 3.7 kbar. Ballou et al. (9) elucidated the helimagnetic structure with a period of about 400 A° of YMn_2, which is consistent with an angle modulation of the antiferromagnetic structure, based on the results of neutron diffraction experiments and NMR spectra arising from a perturbation of the helix by the magnetocrystalline anisotropy.

It was observed that the absorption of hydrogen in YMn_2 or decrease in temperature causes change of high symmetry C15 structure. Fuji et al.(10) have reported

that up to x = 3.5, YMn_2H_x exhibits as solid solution of hydrogen in C15 structure. The cell parameters at room temperature continuously increases with increasing x. For $3.5 < x < 4$, a two phase range with the mixture of cubic and rhombohedral phases exists. For $4 < x < 4.3$, YMn_2D_x exhibits a single phase hydride with a rhombohedral structure (11). Latroche et al. performed neutron diffraction studies of YMn_2D_x ($1 \leq x \leq 4.5$) at temperatures above magnetic transition and reported that the deuterium occupies only the A_2B_2 sites in this range of concentration (12).

The magnetic ordering temperatures T_N of YMn_2H_x compounds (x = 0.5, 2 and 3) increases with increasing x (13). Figiel et al. (14) attributed this deviating behavior to an increase in Mn–Mn distances during hydrogenation. This causes the increasing localization of more stable Mn moments resulting in the suppression of the spin fluctuations. Consequently, the volume anomalies of YMn_2H_x compounds at T_N decrease with increasing x. Some works on hydrogen induced phase transitions of YMn_2H_x $0 < x < 1.2$ were also done by Figiel et al. (14). In their studies, the phase transitions were interpreted in terms of Mn–Mn magnetic interactions which depend on the lattice expansion caused by hydrogen.

From the above discussion it is clear that the magnetic properties of these compounds are very sensitive to Mn–Mn distances. It can be expected that progressive filling of the Mn d-band by electrons derived from hydrogen/deuterium which enter the metallic lattice sites in the form of proton will also influence magnetic structure of YMn_2. Moreover, if some hydrogen or deuterium ordering occurs, it will change, to a certain extent, the magnetic interaction between Mn atoms. Therefore, it could influence the magnetic order not only by varying the lattice constant but also by changing the local environment of the Mn atoms and by inducing distortions in the metal lattice (15). Based on previous works, a phase diagram can be proposed for YMn_2H_x and YMn_2Dx systems $0 \leq x \leq 4.2$ (14,16).

The aim of the present work was to investigate possible existence of the single-phase YMn_2D_x compounds with higher concentration of deuterium $x \geq 4.5$ and, if such

existence is confirmed, to determine their properties. It was already proved that the application of high deuterium pressure can be effectively used for synthesis of novel hydrides in several Laves intermetallic compounds (17). As we expected, we have also succeeded to synthesize new deuteride and in order to identify its structure and characterize its magnetic properties, the powder X-ray diffraction (XRD), Mn X-ray absorption near edge structure (XANES) and magnetization measurements were carried out.

高壓設備架設 (Setup of high pressure equipment)

We have created a very good high pressure synthesis facility in our department which is st of its kind in Taiwan. With this we can synthesize novel materials which are not be able to preparedin atmospheric pressure condition. Also it is possible to find out different kinds of novel high pressure phases under different high pressure conditions with this facility. We are the leaders in Taiwan in such kind of high pressure research.

We have setup three different kinds of high pressure equipments to operate in different temperature and pressure conditions. These are discussed in the following sections.

1. High pressure range:

Fig 1. Pressure intensifier and multiplicator

It contains three important sections as follows:

(i) Pressure intensifier:

a. Basic functions:

Main function of this section is to intensify the hydrogen pressure up to 1000 atm from cylinder pressure. Also this is useful to control the pressure at lower levels even below cylinder pressure. So it acts as a key control system upto a pressure of 1000 atm. Hydrogen cylinder is connected to the multiplicator of pressure intensifier through heavy copper capillary tube which can withstand very high pressures at the order of 1.5 GPa. Metallic ferrules and rubber sealing were used to avoid any leakage near joints.

b. Construction:

It contains a cylinder piston arrangement where hydrogen gas is compressed and fed into the system through multiplicator. Multiplicator is used to split the reactor and hydrogen cylinder by two valves. The pressure of this intersifier is measured by a pressure gauge mounted near hand press which is the pressure inside the reactor also.

c. Working:

Hydrogen cylinder is opened and the gas allowed entering into the intensifier through multiplicator. Hydrogen cylinder and inlet valve in multiplicator are closed and the pressure is increased to the required pressure by pumping the hand pump. During pumping outlet valve of multiplicator kept open to allow the pressurized hydrogen into the reactor. After attaining the required pressure in the reactor, reactor is disconnected from by closing valve near reactor head.

(ii) High pressure piston-cylinder and reactor:

(a) Basic function:

High pressure piston-cylinder is used to increase the hydrogen pressure to a higher range above 1000 atm to a maximum of 15000 atm. Reactor is used to synthesize the samples.

(b) Construction:

Both of these two sections assembled in a single unit with protecting shield as shown in Fig 1. The whole assembly is mounted on a heavy iron base and the piston is connected hydraulically to a hand press which is used to pump the hydrogen to a high pressure.

Reactor is made up of heavy walled beryllium bronze material with a small cylindrical hole in the centre to accommodate sample cells and the piston from the upper side. Lower side is closed by a stopper made up of the same material. Normally material of construction for high hydrogen pressure is beryllium bronze because of hydrogen embrittlement property of stainless steel. Upto 1000 atm pressure stainless steel can be

conveniently used without any problem. Beyond such pressure it is very difficult to maintain a smooth surface of the stainless steel. High pressure hydrogen will penetrate into stainless and start destroying the surface as well as inner structure of stainless steel which will result in the amorphisation of stainless steel.

(c) Working:

After reaching 1000 atm hydrogen pressure from pressure intensifier it is disconnected from the reactor and further increase of pressure is done by high pressure piston-cylinder connected directly to the reactor. Upto four sample cells are kept inside the reactor cylinder and the pressure is slowly raised to the required pressure level.

(iii) Heating coil:

In this high pressure range equipment external heating coil is used to heat up the reactor. Heating coil is covered around the thick walled beryllium bronze and connected to the temperature control device. Thermocouple is connected to the control device and the sensor is inserted near central cylindrical reactor. Maximum temperature attained is about 300 ºC in this setup.

2. Medium pressure range:

It contains only two sections that are pressure intensifier and main reactor.

Pressure intensifier is the same as in the above said high pressure range set up. It can operate upto a pressure of 1000 atm only. Reactor is made up of stainless steel cylinder which is connected to a multiplicator. Multiplicator is further connected to vacuum line and hydrogen cylinder through pressure intensifier. Pressure inside the rector is measured by a small pressure gauge which is used to measure both vacuum as well as pressure upto maximum pressure of 10 atm. After that pressure will be measured by big pressure gauge which is situated near hand press. The reactor assembly is shown in Fig. 2. Cooling water circulation was provided in-between sample and multiplicator to avoid heating up of multiplicator.

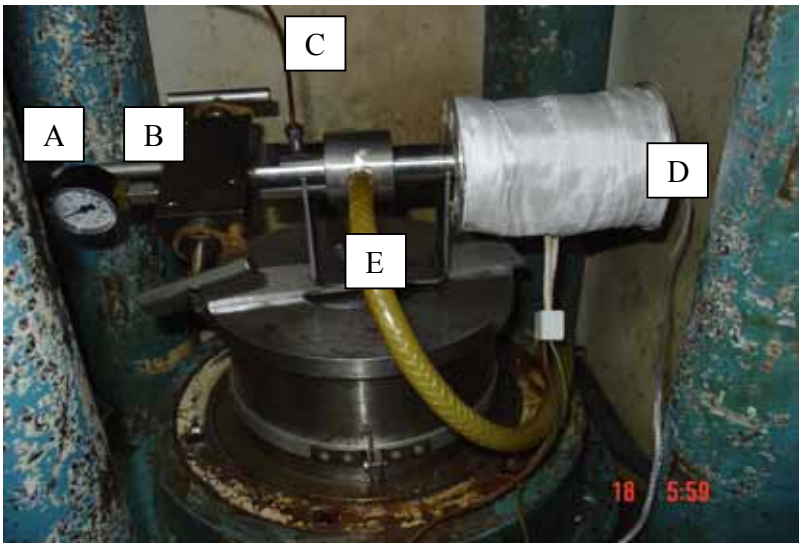

A. Pressure gauge B. Multiplicator C. Capillary D. External heater E. Cooling water circulation

Fig 2. Experimental setup for high pressure synthesis

3. Low pressure and high temperature setup:

In this equipment also pressure intensifier is used to increase the pressure in the reactor as in the case of medium pressure range equipment. But the heating system is entirely different from the above two kinds. It contains a small tiny ceramic wounded coil which is used for the sample vessel holder. Inside the ceramic heated small sample cells will be kept and heated. Very near to sample cell bottom one small thermocouple will be made and the ends of wires will be taken out through stopper to multimeter.

The whole assembly is carefully arranged and kept inside the steel tube with tight sealings. Hydrogen gas will be passed through a small threaded hole by copper capillary from the pressure intensifier.

實驗設備操作方法 (General operation of the equipment)

The samples were loaded into sample cells and closed with threaded covers, placed into the reactor. Cooling water circulation was switched on to avoid heating up of multiplicator. The whole assembly was mounted on protected solid base with heavy

transparent windows. Temperature was slowly increased to 100°C and the sample case is evacuated with vacuum pump for over night. The heater was switched off and the temperature is lowered down to ambient temperature.

Hydrogen pressure was slowly increased from atmospheric pressure to a very low pressure. If absorption is observed periodically pressure level is maintained at low pressure until get saturation. After the saturation point again hydrogen is charged from the cylinder and pressure is increased slowly upto 100 atm and maintained upto two days to complete the absorption. Temperature is slowly increased from room temperature to 100°C and pressure maintained for about an hour to monitor any further absorption. Hydrogen pressure increased slowly and steadily to get maximum hydrogen absorption. Absorption time, pressure and temperature will vary depending on the nature of the sample. After completion of the reaction rector is cooled down to room temperature without disturbing the pressure. On attaining room temperature hydrogen pressure is slowly reduced in steps to the atmospheric pressure over a period of four to five hours.

Immediately after the discharge of the samples they should be preserved in glove or in liquid nitrogen to avoid any loss of hydrogen from the sample due to desorption phenomenon.

實驗 (Experimental Section)

The YMn_2 sample was prepared by induction melting of the pure components (yttrium, 99.9%; manganese, 99.99%) in a water-cooled copper crucible under vacuum then under argon atmosphere to avoid sublimation of manganese (18, 19). In order to prevent the precipitation of Y_6Mn_{23} compound, a 3–5% yttrium excess was added to obtain a single-phase YMn_2 compound. To ensure good homogeneity, the sample was melted five times and annealed for 11 days at 800 ºC.

The homogeneity of the sample was checked by metallographic examination and the composition was analyzed by electron microprobe analysis (EMPA). The powder X-ray diffraction was performed on a PW1710 Philips diffractometer with Cu Ka radiation (λ = 1.5406 Å) and the XRD pattern was successfully indexed as a cubic Fd-3m space group with cell parameter a = 7.681 Å.

About 8 g of the alloy ingot were ground mechanically under argon atmosphere and then sieved for the grain size less than 36 mm. Samples were located in a high pressure apparatus described elsewhere (20) and treated at 100 ºC in vacuum before deuterium charging. Without this treatment, the presence of water adsorbed on the surface of the alloy affects the penetration of deuterium into the bulk (17). The deuterization was performed at pressures of 1.7 kbar of deuterium and temperatures of 200 ºC for 12 h. After the apparatus was cooled down to room temperature, the deuteride was discharged and immediately stored in liquid nitrogen for further investigations. However, soon it became clear that this new deuteride is very stable and can be preserved in ambient conditions without any changes.

Density measurements have been performed using a volumetric method with an Accupyc 1330 Picnometer from Micromeritics Company.

X-ray diffraction (XRD) analyses were carried out with a Brucker diffractometer with Cu Kα radiation. Data for the Rietveld refinement were collected in the 2θ range 10–120º with a step size of 0.02º and a count time of 10 seconds per step. The lattice image of the sample was obtained by high resolution transmission electron microscopy (HRTEM; JEOL 4000EX). The samples for the microscopy were dispersed in alcohol before being transferred to the carbon coated copper grids. The magnetization measurements were done by superconducting quantum interference device (SQUID) magnetometer (Quantum Design).

Density measurements have been performed using a volumetric method with an Accupyc 1330 Picnometer from Micromeritics Company. The neutron powder diffraction (NPD) patterns of the deuteride have been registered at 2 K and 80 K on the 3T2 diffractometer and from 1.4 K to 290 K on the G4.1 diffractometer at the Laboratoire Léon Brillouin (LLB) at Saclay. For the 3T2 experiment the wavelength was 1.225 Å and the angular range $6\ ^\circ < 2\theta < 125\ ^\circ$ with a step of 0.05 °. For the G4.1 experiments the wavelength was 2.427 Å and the angular range was $2\ ^\circ < 2\theta < 82\ ^\circ$ with a step of 0.1°. The deuteride sample was contained in a vanadium sample holder. All the XRD and NPD patterns were refined with the Rietveld method, using the Fullprof program (15).

Differential Scanning Calorimetry (DSC) was performed on TA-Q100 DSC apparatus from TA instrument. The samples were placed in aluminum pan under argon

atmosphere. The experiments were performed from 313 K to temperature ranging from 523 K to 873 K with a rate of 20 K/mn.

Magnetization measurements were performed on a Quantum Design PPMS magnetometer.

The valence of Mn in the synthesized intermetallic deuteride was determined by the X-ray absorption technique. The spectra were obtained using synchrotron radiation with the electron beam energy of 1.5 GeV at NSRRC. They were recorded by measuring the I/I_0 ratio, where I_0 is the intensity of the incident beam. The incident photon flux (I_0) was monitored simultaneously by an ion-chamber which was positioned after the exit slit of the monochromator. The intensity of the transmitted X-ray monitored in the same way was considered as I_0 of the standard metal foil for calibrating the energy of the beam. All the measurements were performed at room temperature. The photon energies were calibrated to an accuracy of 0.1 eV via the theoretical values of the Mn metal K-edge absorption energies. The reproducibility of the absorption spectra of the same sample in different experimental runs was found to be extremely good.

The neutron powder diffraction (NPD) patterns of the deuteride have been recorded at 2 K and 80 K on the 3T2 diffractometer and from 1.4 K to 290 K on the G4.1 diffractometer at the Laboratoire Léon Brillouin (LLB) at Saclay. For the 3T2 experiment the wavelength was 1.225 Å and the angular range $6\ ° < 2\theta < 125\ °$ with a step of 0.05 °. For the G4.1 experiments the wavelength was 2.427 Å and the angular range was $2° < 2\theta < 82\ °$ with a step of 0.1°. The deuteride sample was kept in a vanadium sample holder. All the XRD and NPD patterns were refined with the Rietveld method, using the Fullprof program (21).

結果與討論 (Results and Discussion)

Density measurements lead to a value of d=4.63(1) g/cm^3. This experimental density is in good agreement with the calculated one: d=4.636 g/cm^3 for YMn_2D_6 in a FCC cell with a=6.709 Å and Z= 4 formula units per unit cell.

The powder XRD pattern of the synthesized deuteride and its structural parameters calculated with Rietveld refinement are presented in Fig. 3 and Table 1,

respectively. The values of reliability factors, Rp; Rwp and x calculated from the XRD patern were all acceptable. The pattern could be indexed on the basis of a cubic cell [a = b = c = 6.7093(1) Å, α = β = γ = 90°] and the space group of its crystal structure is F-43m: The crystal structure of the YMn_2D_6 compound plotted with ATOMS software is shown in Fig. 4.

Table 1 Refined atomic positions, unit cell parameter and reliability factor of YMn_2D_6 at 300 K. Some lines are attributed to small amount of Y_2O_3 and $YMn_2D_{4.5}$

Atoms	*x*	*y*	*z*	Wyckoff	Uiso (Å^2)
Y	0.00	0.00	0.00	4a	3.131
Mn(1)	0.50	0.50	0.50	4b	1.436
Mn(2)	0.25	0.25	0.25	4c	1.436
Lattice parameters	Reliability factors				
Space group: *F*-43*m* (216)	$R_p = 10.7\%$				
$a = b = c = 6.7093(1)$Å	$R_{wp} = 13.4\%$				
$\alpha = \beta = \gamma = 90°$	$\chi^2 = 2.41$				

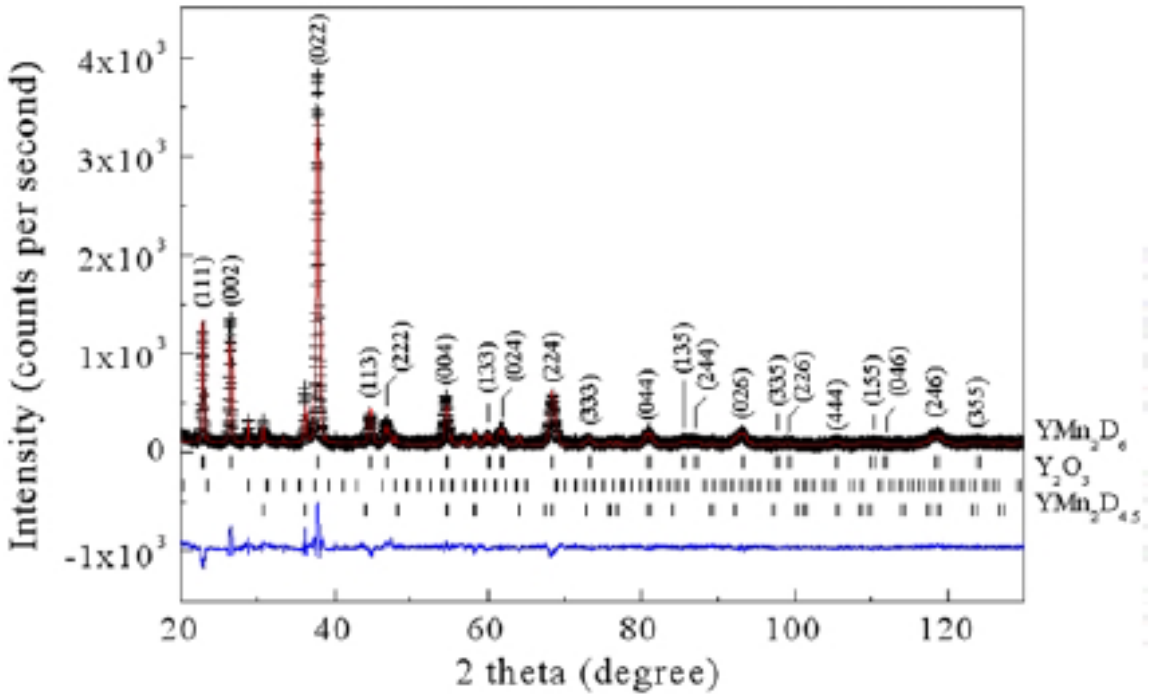

Fig. 3. Rietveld fits to powder XRD data of YMn_2D_6 with F-43m space group. Observed (cross) and calculated (solid line) intensities are shown with the difference at the bottom.

In the C15 type of structure, three kinds of tetrahedral interstitial sites are available for deuterium occupation: AB_3, A_2B_2 and B_4. Experimentally, it has been found that A_2B_2 sites are the most favorable for deuterium bonding, thus they should be filled first. The possibility of filling other two sites, however, could not be excluded, (22, 23) especially when the deuterium content is higher. Moreover, it has been proposed that filling into AB_3 sites might induce a rhombohedral distortion of the host structure (18). However, the crystal symmetry of the YMn_2D_6 is not directly related to the C15 structure. Formation of YMn_2D_6 is accompanied with strong rearrangement of both yttrium and manganese atoms. Also the sites available for deuterium can be very different from A_2B_2, AB_3 and B_4 present in the C15 lattice. For instance we can distinguish A_3B sites in each corner of the unit cell.

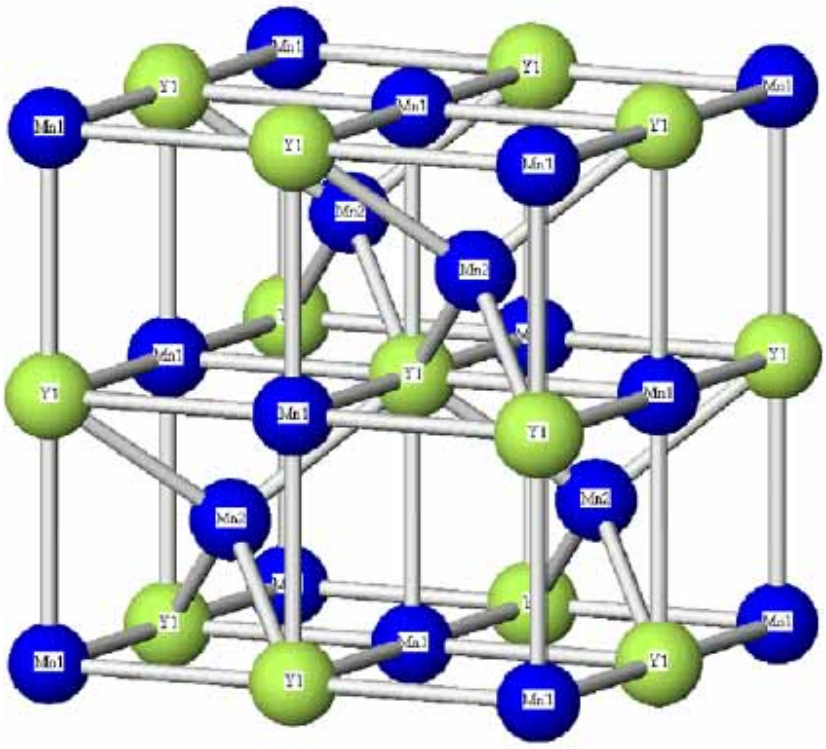

Fig. 4. Crystal structure of the YMn_2D_6 with cubic unit cell (space group: F- 3m).

Fig. 5 shows the lattice image by HRTEM along the [001] zone-axis direction of the cubic crystal system corresponds to its ab plane. This photo also indicates a high crystallinity of the synthesized YMn_2D_6 compound.

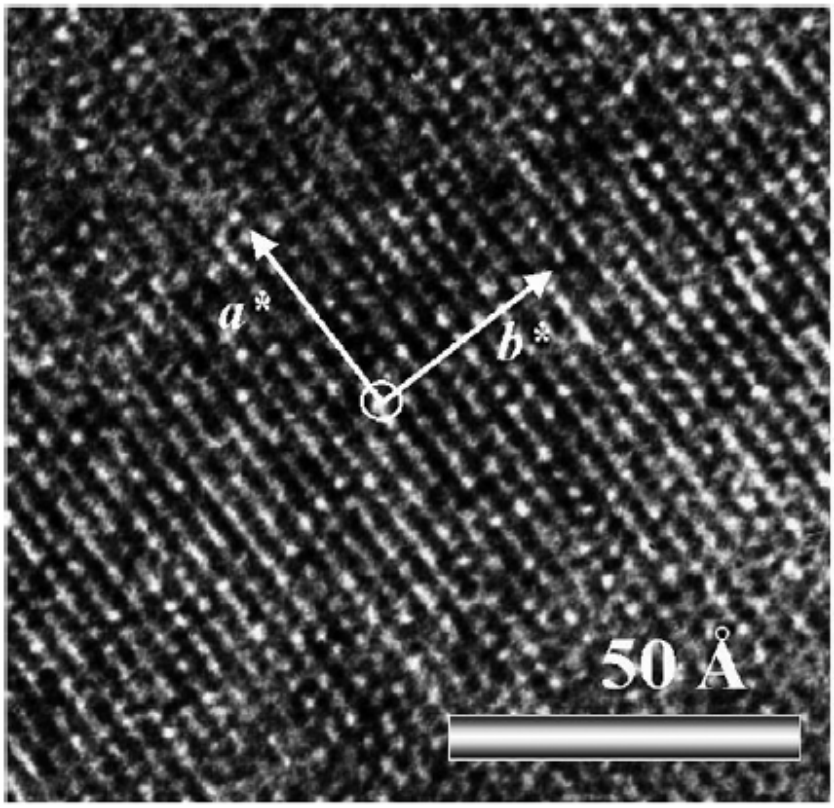

Fig. 5. HRTEM lattice image recorded along the [001] zone-axis direction of YMn_2D_6.

X-ray energies are sufficiently high to eject, via the photoelectric effect, one or more core electrons from an atom. Each core electron has a well-defined binding energy, and when the energy of the incident X-ray is varied across one of these energies, there is an abrupt increase in the absorption coefficient. This is the so-called 'absorption edge' of the element. Absorption edges are named according to the electron of which shell is excited, for example, K = 1s; L_I = 2s, $L_{II,III}$ = 2p, etc. The Mn K-edge XANES spectra of the YMn_2 and YMn_2D_6 compounds are shown in Fig. 6. The Mn foil was used as a reference. Knowing reference spectrum at the absorption edge, it is possible to use it as a fingerprint of the valence and site symmetry, so to characterize the investigated sample.

In other words, although the differences between the energy values (E_0) corresponding to $\mu x = 0.5$ can usually be used to determine the valences of metals in their different compounds; the comparison should be applied based on the same or at least

fairly similar structural coordination environment. It is very important to keep this point in mind as we examine these spectra. Therefore, as shown in Fig. 4, we proposed that the E_0 at such little different energy values was attributed to the different chemical environment of Mn. It is more plausible to determine the valence of Mn based on the energy value of the onset of XANES spectrum (as the arrow A in Fig. 4 shows). Viewed in this light, the valence of Mn in the intermetallic alloy and its deuteride can be regarded as the same metallic state as that of Mn foil.

In the case of K-edge XANES spectrum, the X-ray absorption of a 3d transition metal is mainly due to the excitation process of its 1 s core electron to higher 4p manifold electronic states. For L-edge XANES spectrum, the absorption corresponds to the 2p to 3d transition. The d electrons are more shielded from the chemical environment than p electrons and therefore in greater degree have retained their atomic character. As a consequence, it is suggested that the L-edge XANES spectrum has less interference from the site symmetry. The Mn L edge XANES spectra of the YMn_2 and YMn_2D_6 are shown in Fig. 5. The spectra show two separated broad multiple structures arising from the spin-orbital splitting of Mn 2p electronic energy levels. The former and latter peaks correspond to $2p_{3/2}$ to 3d and $2p_{1/2}$ to 3d transitions, named L_{III} and L_{II}-edge, respectively.

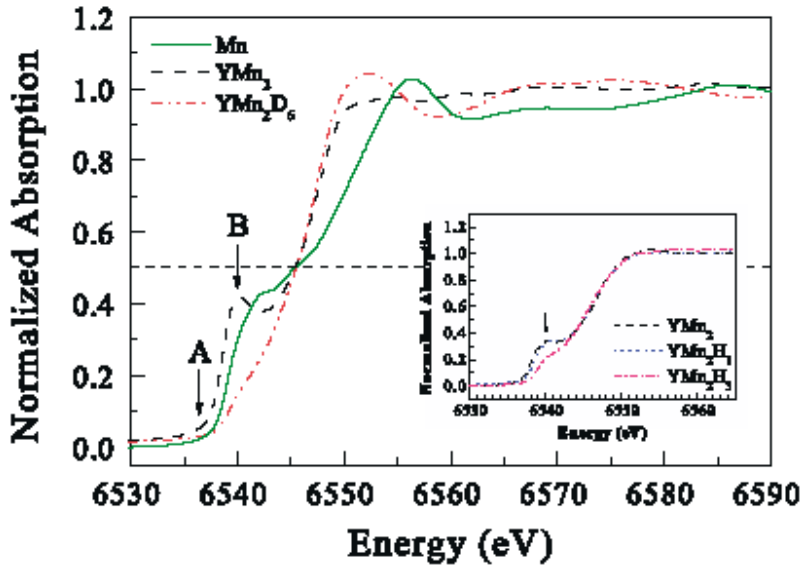

Fig. 6. Normalized Mn K-edge XANES spectra of the YMn_2 and YMn_2D_6 compounds and that of the standard sample (Mn foil). For reference the results of YMn_2, YMn_2H and YMn_2H_3 are shown in the inset.

Using the integrated area under the L_{III}- and L_{II}-edge XANES spectra it is even possible to quantify the changes in d-band occupancy. When we consider the role of deuterium in the host, the state of Mn influenced by complicate electronic interactions becomes more open to question. After careful comparison, it seems that the L-edge spectra of these two samples do not differ markedly. It can be then concluded that the manganese is metallic and alloyed with yttrium. An obvious change in the intensity of the pre-edge peak located at 6540 eV, as shown by arrow B in Fig. 6, is observed. For the YMn_2D_6 compounds this peak even completely vanished. This result is in agreement with tendency observed for smaller hydrogen concentration (inset in Fig. 6). As we mentioned above, according to the dipolar selection rules, the K-edge corresponds to an electronic transition from 1 s core state to empty p state and the XANES spectrum probes the empty projected local electronic density of p state (24). The Mn 4p states are hybridized with partially empty Mn 3d states, i.e. the pre-edge structure is related to the hybrid p–d states. Since the Mn 3d states are dominant at the Fermi level, the dramatic change of the pre-edge peak might indicate a reduction of the number of 3d holes due to the shift of 3d band below the Fermi level after hydrogen absorption (25).

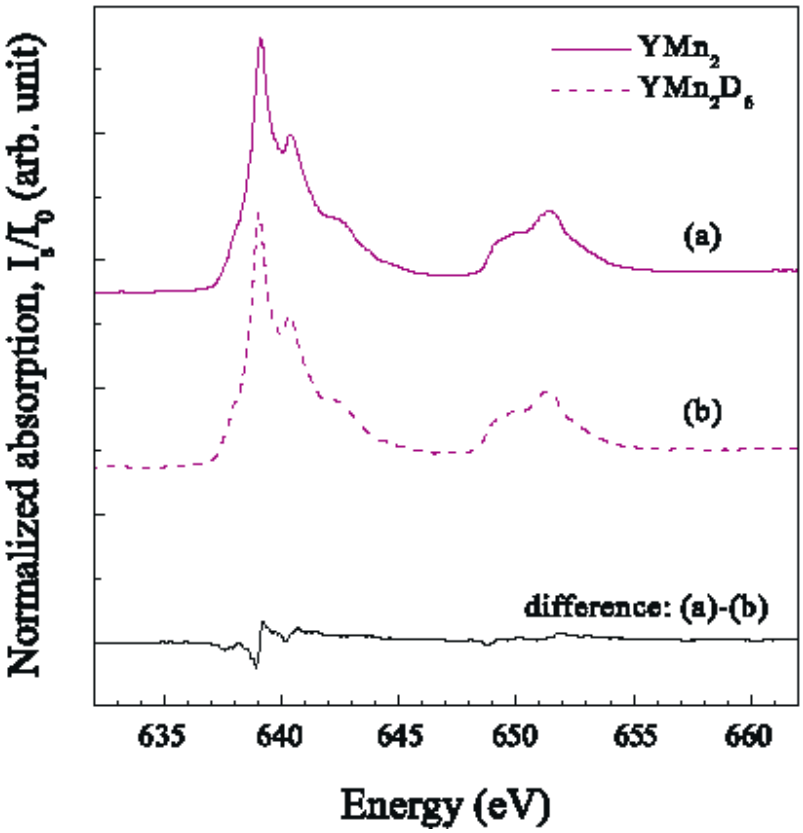

Fig. 7. Normalized Mn L-edge XANES spectra of YMn_2 and YMn_2D_6

The magnetization curves of the YMn_2 and YMn_2D_6 compounds as a function of temperature were shown in Fig. 8. The absorption of deuterium results in the two-orders enhanced magnetic moment of Mn and there is a rapid increase of magnetization of the YMn_2D_6 compound when temperature decreases from 120 K down to 5 K. In Fig. 9 the magnetization loops for the YMn_2 and YMn_2D_6 compounds are compared. The magnetization curves measured at 5 K show a larger magnetic hysteresis for YMn_2D_6 than YMn_2. It was found that the deuteride exhibits magnetic moment higher than its parent alloy (YMn_2). The magnetization of both, YMn_2 and YMn_2D_6 samples was not saturated at magnetic field up to 5 T.

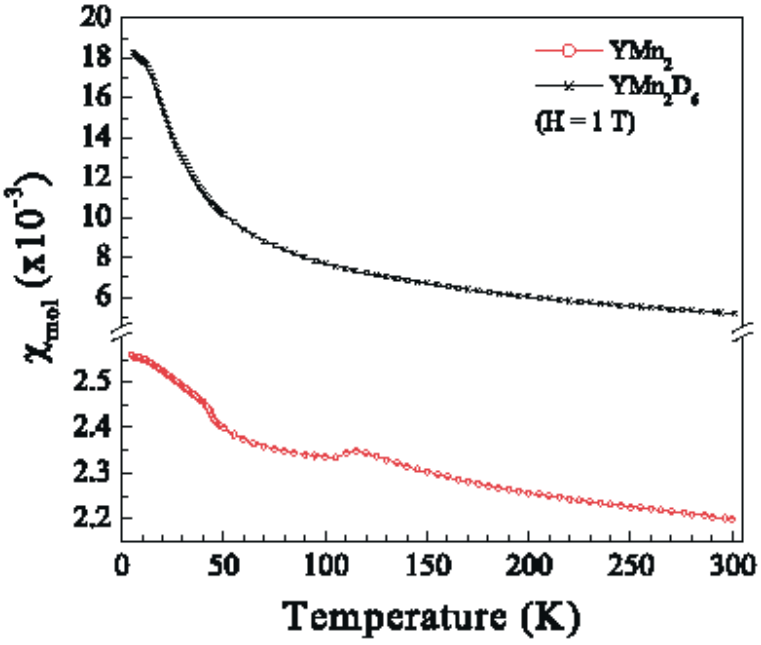

Fig. 8. Temperature dependence of magnetization of YMn_2 and YMn_2D_6 at a magnetic field of 1 T.

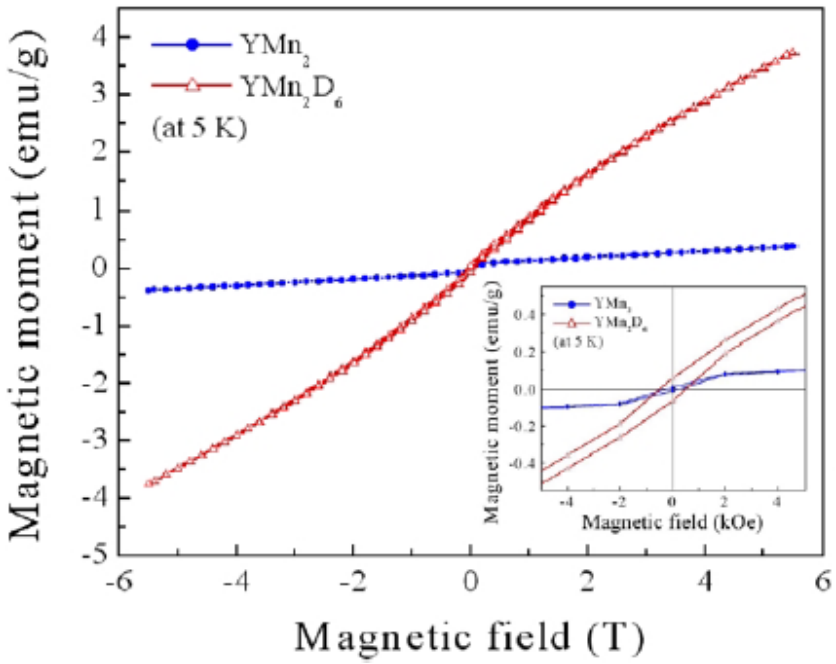

Fig. 9. Magnetization loops of YMn_2 and YMn_2D_6 measured at 5 K (H = 25 to 5 T).

結論**(Conclusions)**

The novel intermetallic deuteride YMn_2D_6 was successfully synthesized under high deuterium pressure conditions. The structure of YMn_2D_6 (F-43m) differs dramatically from C15 symmetry (Fd-3m) of the parent material. Such a great rearrangement of the metal lattice due to deuterium absorption is rather exceptional for C15 Laves phases. Some chemical and physical properties of YMn_2D_6 were also examined by several analytic methods. X-ray absorption spectroscopy indicates progressive filling of the Mn d band by electrons derived from deuterium which, in ionic form, occupies sites in the metallic lattice. During reaction of deuterium with YMn_2, leading to formation of YMn_2D_6, the changes of electronic structure, crystal symmetry, atomic environment and interatomic distances occur.

計畫成果自評 **(Evaluation of the project)**

We have reached the goals of the research plan, some parts of the results have already been published in scientific journals (26-27). Moreover, we have also presented the outcome of this project in various international conferences (28-33).

參考文獻 **(References)**

1. B. Baranowski, R. Wiśniewski, Bull. Polon. Acad. Sci., 14 (1966), 273
2. S.M. Filipek, B. Baranowski, M.Yoneda, Roczniki Chem., 51 (1977) 2243
3. M. Krukowski, B. Baranowski, Roczn. Chem., 49 (1975) 1183
4. A.E. Dwight, Trans. Am. Soc. Met. 53 (1961) 479.
5. H. Wada, H. Nakamura, K. Yoshimura, M. Shiga, Y. Nakamura, J. Magn. Magn. Mater. 70 (1987) 134.
6. T. Okamoto, H. Nagata, H. Fujii, Y. Makihara, J. Magn. Magn. Mater. 70 (1987) 139.
7. M. Shiga, H. Wada, H. Nakamura, K. Yoshimura, Y. Nakamura, J. Phys. F 17 (1987) 1781.
8. G. Oomi, T. Terada, M. Shiga, Y. Nakamura, J. Magn. Magn. synthesis, J. Jurczak, B. Baranowski, editors, Elsevier, Mater. 70 (1987) 137.

9. R. Ballou, J. Deportes, R. Lemaire, Y. Nakamura, B. Ouladdiaf, J. Magn. Magn. Mater. 70 (1987) 129.
10. H. Fuji, M. Saga, T. Okamoto, J. Less-Common Met. 130 (1987) 25.
11. J. Przewoznik, V. Paul-Boncour, M. Latroche, A. Percheron- Guegan, J. Alloys Compd. 225 (1995) 436.
12. M. Latroche, V. Paul-Boncour, J. Przewoznik, A. Percheron-Guegan, F. Bouree-Vigneron, J. Alloys Compd. 231 (1995) 99.
13. H. Figiel, A. Lindbaum, Cs. Kapusta, E. Gratz, J. Alloys Compd. 217 (1995) 157.
14. H. Figiel, J. Przewoznik, V. Paul-Boncour, A. Lindbaum, E. Gratz, M. Latroche, M. Escorne, A. Percheron-Gue´gan, P. Mietniowski, J. Alloys Compd. 274 (1998) 29.
15. I.N. Goncharenko, I. Mirebeau, A.V. Irodova, E. Suard, Phys. Rev. B 56 (1997) 2580.
16. J. Przewoznik, J. Zukrowski, K. Krop, J. Magn. Magn. Mater. 140 (1995) 807.
17. S.M. Filipek, V. Paul-Boncour, A. Percheron-Guegan, I. Jacob, I. Marchuk, M. Dorogova, T. Hirata, Z. Kaszkur, J. Phys.: Condens. Matter 13 (2001) 475.
18. M. Latroche, V. Paul-Boncour, A. Percheron-Guegan, F. Bouree-Vigneron, J. Alloys Compd. 274 (1998) 59.
19. M. Latroche, V. Paul-Boncour, A. Percheron-Gue gan, F. Boure´e-Vigneron, G. Andre´, J. Solid State Chem. 154 (2000) 398.
20. B. Baranowski, S.M. Filipek, High pressure chemical synthesis, J. Jurczak, B. Baranowski, editors, Elsevier, Amsterdam, pp. 55–100.
21. Rodríguez-Carvajal J 1990 in proceedings of *Congr. Int. Union of Crystallography*, p. 127.
22. D. Fruchart, A. Rouault, C.B. Shoemaker, D.P. Shoemaker, J. Less-Common Met. 73 (1980) 363.
23. A.V. Irodova, O.A. Lavrova, G.V. Laskova, L.N. Padurets, Sov. Phys. Solid State 24 (1982) 22.
24. V. Paul-Boncour, A.P. Gue´gan, J. Alloys Compd. 293–295 (1999) 237.

25. S. Matar, V. Paul-Boncour, Proceedings of the groupement francais de spectroscopie mo¨ssbauer, Juins, Bordeaux, 1998.
26. C.Y. Wang, V.P. Boncour, C.C. Kang, R.S. Liu, S.M. Filipek, M. Dorogova, I. Marchuk, T.Hirata, A.P. Guegan, H. S. Sheud, L. Y. Jang, J.M. Chen, H.D. Yang, Solid State Commun. 130 (2004) 815.
27. V. Paul-Boncour, S.M. Filipek, M. Dorogova, F. Bourée, G. André, I. Marchuk, A. Percheron-Guégan, R. S. Liu, J. Solid State Chem. 178 (2005) 356.
28. Characterization of several Laves phase hydrides recently synthesized under high hydrogen pressure, S.M. Filipek, V. Paul-Boncour, H. Sugiura, Ru-Shi Liu F. Bourée, G. Wiesinger, T. Hirata, A. Percheron-Guégan, I. Marchuk, M. Dorogova; Joint 19th AIRAPT - 41st EHPRG International Conference on High Pressure Science and Technology, Bordeaux, Francja, 7-11 July, 2003
29. A new hydride phase of YMn_2 synthesized under high hydrogen pressure and its characterization, S. M. Filipek, V. Paul-Boncour, C. Y. Wang, R. S. Liu, T. Hirata, I. Marchuk, M. Dorogova, A. Percheron-Guegan, H.-S. Sheu, L.-Y. Jang, J. M. Chen and H. D. Yang, Joint 19th AIRAPT - 41st EHPRG International Conference on High Pressure Science and Technology, Bordeaux, Francja, 7-11 July, 2003
30. Properties of Novel Hydrides Synthesized under High Hydrogen Pressures from *C*15 Laves Phases S.M. Filipek, V. Paul-Boncour, H. Sugiura, R.S. Liu and I. Marchuk, III International Conference, "Phase Transformations under High Pressures", HPP-2004, June 1-3, 2004, Chernogolovka.
31. High Pressures Studies on Hydrides of Selected Manganese Alloys, H. Sugiura, S.M. Filipek, V. Paul-Boncour, I. Marchuk, R.S. Liu M. Dorogova, S.I. Pyun, IV International Conference "Hydrogen Treatment of Materials" May 17-21. 2004 Donieck (Ukraine).
32. Studies on the Magnetic Properties and Low-Temperature Specific Heat of a Novel YMn_2D_6 Compound Synthesized under High Pressure of Gaseous Deuterium Chien-Yuan Wang, Chun-Bo Tsai, Yang-Yuan Chen, Valerie Paul-Boncour, Chia-Cheng Kang, Ru-Shi. Liu, Stanislaw M. Filipek, Maria Dorogova,

Iryna Marchuk, International Conference on Metal Hydrogen Systems, MH2004. 5 – 10 Sept. 2004, Krakow POLAND.

33. Low-Temperature Specific Heat and Magnetic Properties of a Novel YMn_2D_6 Deuteride, C. Y. Wang, C. B. Tsai, Y-Y. Chen, V. Paul-Boncour, C-C.Kang, R-.S. Liu, S. M. Filipek, M. Dorogova, I. Marchuk, A. Percheron-Guegan, and H-D. Yang International Conference on Metal Hydrogen Systems, MH2004. 5 – 10 Sept. 2004, Krakow POLAND.

(附錄一)
行政院國家科學委員會補助專題研究計畫

利用高壓合成新材料及其特性分析(中波國合計畫)
發表論文清單

1. **C.Y. Wang, V.P. Boncour, C.C. Kang, R.S. Liu, S.M. Filipek, M. Dorogova, I. Marchuk, T.Hirata, A.P. Guegan, H. S. Sheud, L. Y. Jang, J.M. Chen, H.D. Yang, Solid State Commun. 130 (2004) 815.**

2. **V. Paul-Boncour, S.M. Filipek, M. Dorogova, F. Bourée, G. André, I. Marchuk, A. Percheron-Guégan, R. S. Liu, J. Solid State Chem. 178 (2005) 356.**

Available online at www.sciencedirect.com
SCIENCE DIRECT
Solid State Communications 130 (2004) 815–820
solid state communications
www.elsevier.com/locate/ssc

The novel YMn_2D_6 deuteride synthesized under high pressure of gaseous deuterium

Chien-Yuan Wang[a], Valerie Paul-Boncour[b], Chia-Cheng Kang[a], Ru-Shi Liu[a,*], Stanislaw M. Filipek[c,*], Maria Dorogova[c], Iryna Marchuk[c], Toshiya Hirata[c], Annick Percheron-Guegan[b], Hwo-Shuenn Sheu[d], Ling-Yun Jang[d], Jin-Ming Chen[d], Hung-Duen Yang[e]

[a]*Department of Chemistry, National Taiwan University, Taipei, Taiwan, ROC*
[b]*Laboratoire de Chimie Métallurgique des Terres Rares, CNRS, Meudon, France*
[c]*Institute of Physical Chemistry, Polish Academy of Science, Warsaw, Poland*
[d]*National Synchrotron Radiation Research Center, Hsinchu, Taiwan, ROC*
[e]*Department of Physics, National Sun Yat-Sen University, Kaohsiung, Taiwan, ROC*

Received 9 February 2004; accepted 22 March 2004 by C.N.R. Rao

Abstract

The novel intermetallic deuteride YMn_2D_6 was synthesized under high deuterium pressure. In order to identify the structure and characterize the magnetic properties of this deuteride the powder X-ray diffraction (XRD), high-resolution transmission electron microscopy (HRTEM), Mn X-ray absorption near edge structure (XANES) and magnetization measurement (SQUID) were carried out. The crystal structure, the chemical state of Mn and the magnetic properties of this novel deuteride were examined and discussed. It should be noted that the structure of YMn_2D_6 (F-43m) differs dramatically from C15 symmetry of the parent material. Such a great rearrangement of the metal lattice due to deuterium absorption is rather exceptional for C15 Laves phase.

PACS: 61.66.Dk; 07.35. + k; 64.70.Kb; 61.10.Ht

Keywords: A. Alloys; B. High-pressure apparatus; C. Solid-solid transitions; D. X-ray absorption spectroscopy

1. Introduction

Under ambient conditions [1] the intermetallic Laves compound YMn_2 has by a cubic C15 crystal structure with Fd-3m space group. It is an itinerant electron antiferromagnet with the Mn moments (μ_{Mn}) of 2.7 μ_B [2] and the Néel temperature (T_N) of ~100 K [3,4]. The results of heat capacity and thermal expansion measurements as a function of temperature indicate that this compound exhibits a first order phase transition at T_N accompanied with a giant volume change of about 5%, which is ascribed to the spontaneous volume magnetostriction due to the collapse of the Mn moment at T_N [4,5]. Another anomalous behavior of YMn_2 is a large thermal expansion coefficient above T_N. Such behavior can be interpreted by a rapid recovery of the amplitude of spin fluctuations with increasing temperature above T_N [6] Oomi et al. [7] found that the magnetism of YMn_2 is very sensitive to external pressure: the onset of magnetic order is not observable at 3.7 kbar. Ballou et al. [8] elucidated the helimagnetic structure with a period of about 400 Å of YMn_2, which is consistent with an angle modulation of the antiferromagnetic structure, based on the results of neutron diffraction experiments and NMR spectra arising from a perturbation of the helix by the

* Corresponding author. Tel.: +886-2-2369-0152 x148; fax: +886-2-2363-6359.
E-mail address: rsliu@ntu.edu.tw (R.S. Liu).

0038-1098/$ - see front matter © 2004 Elsevier Ltd. All rights reserved.
doi:10.1016/j.ssc.2004.03.054

magnetocrystalline anisotropy. Further efforts were done by Nakamura et al., [3–10] who found, by analyzing both the intensity of magnetic peaks and the ^{55}Mn spin-echo NMR spectrum at 4.2 K that the spin axis, i.e. the direction of magnetization, is parallel to the [111] direction. Then the electronic structures of YMn_2 and related compounds were calculated by several theoretical methods being in good agreement with the experimental results [2,11,12].

It was also found that a change of high-symmetry C15 structure (*Fd-3m* space group) of YMn_2 intermetallic compound is induced by absorption of hydrogen or decreasing in temperature. Fuji et al. [13] have shown that up to $x = 3.5$ the YMn_2H_x hydrides are a solid solution of hydrogen in the C15 structure. The cell parameter at room temperature increases continuously with increasing x. For $3.5 < x < 4$, a two-phase range with a mixture of cubic and rhombohedral phases exists. For $4 < x < 4.3$, a single phase hydride with a rhombohedral structure ($R-3m$ space group) was obtained [14]. Latroche et al. [15,16] performed the neutron powder diffraction experiments of YMn_2D_x ($1 \leq x \leq 4.5$) at temperatures above the magnetic transition. They determined the atomic position and site occupation of deuterium finding that only the A_2B_2 sites were occupied in this range of concentration.

The magnetic ordering temperatures (T_N) of YMn_2H_x compounds ($x = 0.5$, 2 and 3) increase with increasing of x [17]. Figiel et al. [18] attributed this deviating behavior to an increase in Mn–Mn distances during hydrogenation. This causes the increasing localization of more stable Mn moments resulting in the suppression of the spin fluctuations. Consequently, the volume anomalies of YMn_2H_x compounds at T_N decrease with increasing of x. Some works on hydrogen induced phase transitions of YMn_2H_x ($0 < x < 1.2$) were also done by Figiel et al. [18]. In their studies, the phase transitions were interpreted in terms of Mn–Mn magnetic interactions in dependence of the lattice expansion caused by hydrogen. Fujii et al. [19] and Goncharenko et al. [20] also proved that YMn_2H_x compounds exhibit a weak ferromagnetic property in the range of $1 < x < 3.5$ while for the rhombohedral phase with $x = 4.3$, an antiferromagnetic state is observed. The YMn_2D_x ($x = 1.15$ and 4.5) compounds have been studied by means of temperature dependent neutron diffraction reported by Latroche et al. [16,21]. They concluded that under ambient pressure, both deuterium ordering and magnetic interactions are intimately related and involve each other, however, which is the first effect to take place is still a question. From their study on YMn_2D_1, it was expected that the magnetic effect is the driving force involving an electronic and geometrical modification of the lattice and that deuterium ordering is a consequence of this rearrangement [22]. Anyhow, it is clear that magnetic properties of these compounds are very sensitive to Mn–Mn distances. It can be excepted that progressive filling of the Mn d-band by electrons derived from hydrogen/deuterium which enter the metallic lattice sites in the form of proton will also influence magnetic structure of YMn_2. Moreover, if some hydrogen or deuterium ordering occurs, it will change, to a certain extent, the magnetic interaction between Mn atoms. Therefore, it could influence the magnetic order not only by varying the lattice constant but also by changing the local environment of the Mn atoms and by inducing distortions in the metal lattice [20]. Based on previous works, a phase diagram can be proposed for YMn_2H_x and YMn_2D_x systems ($0 \leq x \leq 4.2$) [18,23].

The aim of the present work was to investigate possible existence of the single-phase YMn_2D_x compounds with higher concentration of deuterium ($x \geq 4.5$) and, if such existence is confirmed, to determine their properties. It was already proved that the application of high deuterium pressure technique can be effectively used for synthesis of novel hydrides in several Laves intermetallic compounds [24]. As we expected, we have also succeeded to synthesize new deuteride and in order to identify its structure and characterize its magnetic properties, the powder X-ray diffraction (XRD), Mn X-ray absorption near edge structure (XANES) and magnetization measurements were carried out.

2. Experimental section

The YMn_2 sample was prepared by induction melting of the pure components (yttrium, 99.9%; manganese, 99.99%) in a water-cooled copper crucible under vacuum then under argon atmosphere to avoid sublimation of manganese [16,25]. In order to prevent the precipitation of the Y_6Mn_{23} compound, a 3–5% yttrium excess was added for obtaining a single-phase YMn_2 compound. To ensure good homogeneity, the sample was melted five times and annealed for 11 days at 800 °C. The homogeneity of the sample was checked by metallographic examination and the composition was analyzed by electron microprobe analysis (EMPA). The powder X-ray diffraction was performed on a PW1710 Philips diffractometer with Cu K_α radiation ($\lambda = 1.5406$ Å) and the XRD pattern was successfully indexed as a cubic *Fd-3m* space group with cell parameter $a = 7.681(1)$ Å. About 8 g of the alloy ingot were ground mechanically under argon atmosphere and then sieved for the grain size less than 36 μm.

Samples were located in a high pressure apparatus described elsewhere [26] and treated at 100 °C in vacuum before the deuterium charging. Without this treatment, the presence of water adsorbed on the surface of the alloy affects the penetration of deuterium into the bulk [24]. The deuterization was performed at pressures of 1.7 kbar of deuterium and temperatures of 200 °C for 12 h. After the apparatus was cooled down to room temperature, the deuteride was discharged and immediately stored in liquid nitrogen for further investigations. However, soon it became clear that this new deuteride is very stable and can be kept

long time in ambient conditions without any changes. The deuterium content, measured by elemental analyzer (Perkin Elmer 240), corresponds to formula YMn_2D_6.

X-ray diffraction (XRD) analyses were carried out with a Brucker diffractometer with Cu K_α radiation. Data for the Rietveld refinement were collected in the 2θ range 10–120° with a step size of 0.02° and a count time of 10 seconds per step. The lattice image of the sample was obtained by high-resolution transmission electron microscopy (HRTEM; JEOL 4000EX). The samples for the microscopy were dispersed in alcohol before being transferred to the carbon-coated copper grids. The magnetization measurements were done by superconducting quantum interference device (SQUID) magnetometer (Quantum Design).

The valence of Mn in the synthesized intermetallic deuteride was determined by the X-ray absorption technique. The spectra were obtained using synchrotron radiation with the electron beam energy of 1.5 GeV at NSRRC. They were recorded by measuring the I/I_0 ratio, where I_0 is the intensity of the incident beam. According to the attenuation law $I = I_0\exp(-\mu x)$, $\ln(I/I_0)$ is proportional to the absorption function μ. Based on the transmission mode, the thickness x of the sample has to be adjusted such as $\mu x \sim 1$, where μ is the absorption cross-section of the element of interest. The incident photon flux (I_0) was monitored simultaneously by an ion-chamber which was positioned after the exit slit of the monochromator. The intensity of the transmitted X-ray monitored in the same way was considered as I_0 of the standard metal foil for calibrating the energy of the beam. All the measurements were performed at room temperature. The photon energies were calibrated to an accuracy of 0.1 eV via the theoretical values of the Mn metal K-edge absorption energies. The reproducibility of the absorption spectra of the same sample in different experimental runs was found to be extremely good.

3. Results and discussion

The powder XRD pattern of the synthesized deuteride and its structural parameters calculated with Rietveld refinement are presented in Fig. 1 and Table 1, respectively. The values of reliability factors, R_p, R_{wp} and χ [2] calculated from the XRD patent were all acceptable. The pattern could be indexed on the basis of a cubic cell [$a = b = c = 6.7093(1)$ Å, $\alpha = \beta = \gamma = 90°$] and the space group of its crystal structure is F-43m. The crystal structure of the YMn_2D_6 compound plotted with ATOMS software is shown in Fig. 2.

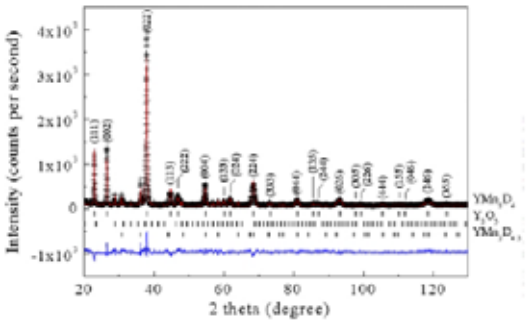

Fig. 1. Rietveld fits to powder XRD data of YMn_2D_6 with F-43m space group. Observed (cross) and calculated (solid line) intensities are shown with the difference at the bottom.

In the C15 type of structure, three kinds of tetrahedral interstitial sites are available for deuterium occupation: AB_3, A_2B_2 and B_4. Experimentally, it has been found that A_2B_2 sites are the most favorable for deuterium bonding, thus they should be filled first. The possibility of filling other two sites, however, could not be excluded, [27,28] especially when the deuterium content is higher. Moreover, it has been proposed that filling into AB_3 sites might induce a rhombohedral distortion of the host structure [16].

However, the crystal symmetry of the YMn_2D_6 is not directly related to the C15 structure. Formation of YMn_2D_6 is accompanied with strong rearrangement of both yttrium and manganese atoms. Also the sites available for deuterium can be very different from A_2B_2, AB_3 and B_4 present in the C15 lattice. For instance we can distinguish A_3B sites in each corner of the unit cell. Therefore, the discussion about filling the sites in this novel F-43m lattice of YMn_2D_6 will be postponed to the next experiment with neutron diffraction.

Table 1
Refined atomic positions, unit cell parameter and reliability factor of YMn_2D_6 at 300 K. Some lines are attributed to small amount of Y_2O_3 and $YMn_2D_{4.5}$

Atoms	x	y	z	Wyckoff	Uiso (Å^2)
Y	0.00	0.00	0.00	4a	3.131
Mn(1)	0.50	0.50	0.50	4b	1.436
Mn(2)	0.25	0.25	0.25	4c	1.436
Lattice parameters	Reliability factors				
Space group: F-43m (216)	$R_p = 10.7\%$				
$a = b = c = 6.7093(1)$Å	$R_{wp} = 13.4\%$				
$\alpha = \beta = \gamma = 90°$	$\chi^2 = 2.41$				

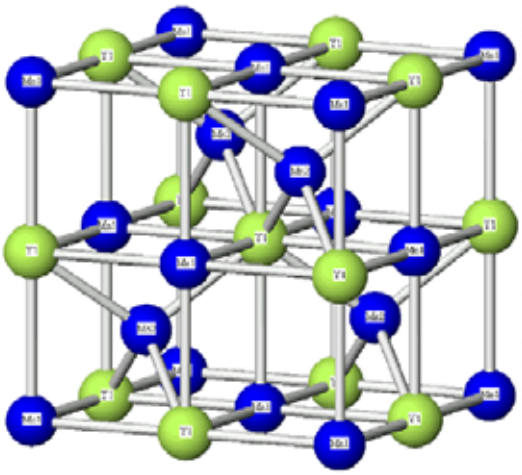

Fig. 2. Crystal structure of the YMn_2D_6 with cubic unit cell (space group: $F\bar{4}3m$).

We believe that neutron diffraction will provide us with data necessary to describe the location of deuterium atoms in YMn_2D_6.

As shown in Fig. 3, the lattice image by HRTEM along the [001] zone-axis direction of the cubic crystal system corresponds to its *ab* plane. This photo also indicates a high crystallinity of the synthesized YMn_2D_6 compound.

X-ray energies are sufficiently high to eject, via the photoelectric effect, one or more core electrons from an atom. Each core electron has a well-defined binding energy, and when the energy of the incident X-ray is varied across one of these energies, there is an abrupt increase in the absorption coefficient. This is the so-called 'absorption edge' of the element. Absorption edges are named according to the electron of which shell is excited, for example, K = 1s; L_I = 2s,$L_{II,III}$ = 2p, etc. The Mn K-edge XANES spectra of the YMn_2 and YMn_2D_6 compounds are shown in Fig. 4. The Mn foil was used as a reference. Knowing reference spectrum at the absorption edge, it is possible to use it as a fingerprint of the valence and site symmetry, so to characterize the investigated sample. In other words, although the differences between the energy values (E_0) corresponding to $\mu x = 0.5$ can usually be used to determine the valences of metals in their different compounds, the comparison should be applied based on the same or at least fairly similar structural coordination environment. It is very important to keep this point in mind as we examine these spectra. Therefore, as shown in Fig. 4, we proposed that the E_0 at such little different energy values was attributed to the different chemical environment of Mn. It is more plausible to determine the valence of Mn based on the energy value of the onset of XANES spectrum (as the arrow A in Fig. 4 shows). Viewed in this light, the valence of Mn in the intermetallic alloy and its deuteride can be regarded as the same metallic state as that of Mn foil. In the case of K-edge XANES spectrum, the X-ray absorption of a 3d transition metal is mainly due to the excitation process of its 1 s core electron to higher 4p manifold electronic states. For L-edge XANES spectrum, the absorption corresponds to the 2p to 3d transition. The d electrons are more shielded from the chemical environment than p electrons and therefore in greater degree have retained their atomic character. As a consequence, it is suggested that the L-edge XANES spectrum has less interference from the site symmetry. The Mn L edge XANES spectra of the YMn_2 and YMn_2D_6 are shown in Fig. 5. The spectra show two separated broad multiple structures arising from the spin-orbital splitting of Mn 2p electronic energy levels. The former and latter peaks correspond to $2p_{3/2} \rightarrow 3d$ and $2p_{1/2} \rightarrow 3d$ transitions are named L_{III} and L_{II}-edge, respectively. Using the integrated

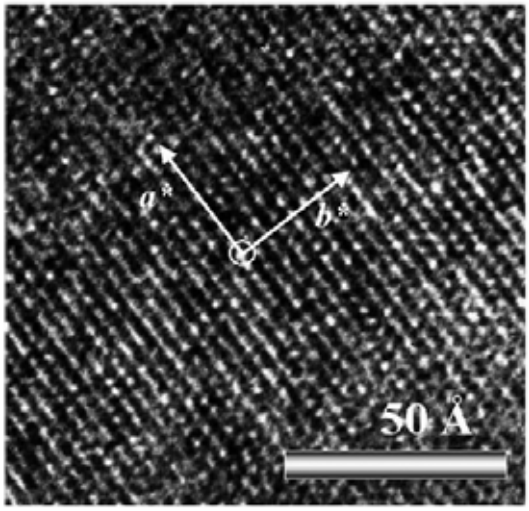

Fig. 3. HRTEM lattice image recorded along the [001] zone-axis direction of YMn_2D_6.

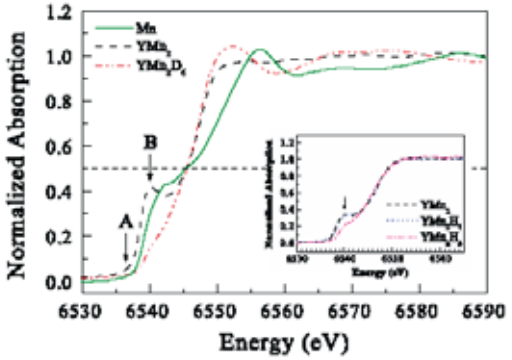

Fig. 4. Normalized Mn K-edge XANES spectra of the YMn_2 and YMn_2D_6 compounds and that of the standard sample (Mn foil). For reference the results of YMn_2, YMn_2H_4 and YMn_2H_5 are shown in the inset.

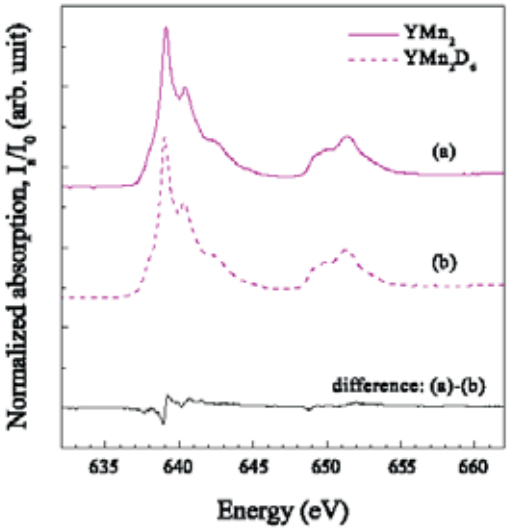

Fig. 5. Normalized Mn L-edge XANES spectra of YMn_2 and YMn_2D_6.

area under the L_{III}- and L_{II}-edge XANES spectra it is even possible to quantify the changes in d-band occupancy. When we consider the role of deuterium in the host, the state of Mn influenced by complicate electronic interactions becomes more open to question. After careful comparison, it seems that the L-edge spectra of these two samples do not differ markedly. It can be then concluded that the manganese is metallic and alloyed with yttrium. An obvious change in the intensity of the pre-edge peak located at 6540 eV, as shown by arrow B in Fig. 4, is observed. For the YMn_2D_6 compounds this peak even completely vanished. This result is in agreement with tendency observed for smaller hydrogen concentration (inset in Fig. 4). As we mentioned above, according to the dipolar selection rules, the K-edge corresponds to an electronic transition from 1 s core state to empty p state and the XANES spectrum probes the empty projected local electronic density of p state [29]. The Mn 4p states are hybridized with partially empty Mn 3d states, i.e. the pre-edge structure is related to the hybrid p–d states. Since the Mn 3d states are dominant at the Fermi level, the dramatic change of the pre-edge peak might indicate a reduction of the number of 3d holes due to the shift of 3d band below the Fermi level after hydrogen absorption [30].

The magnetization curves of the YMn_2 and YMn_2D_6 compounds as a function of temperature were shown in Fig. 6. The absorption of deuterium results in the two-orders enhanced magnetic moment of Mn and there is a rapid increase of magnetization of the YMn_2D_6 compound when temperature decreases from 120 K down to 5 K. In Fig. 7 the magnetization loops for the YMn_2 and YMn_2D_6 compounds are compared. The magnetization curves measured at 5 K show a larger magnetic hysteresis for YMn_2D_6 than YMn_2. It was found that the deuteride exhibits magnetic moment

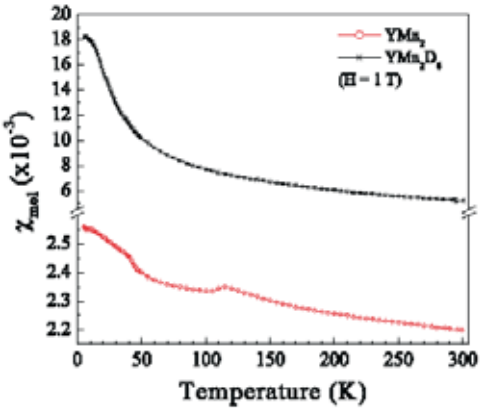

Fig. 6. Temperature dependence of magnetization of YMn_2 and YMn_2D_6 at a magnetic field of 1 T.

higher than its parent alloy (YMn_2). The magnetization of both, YMn_2 and YMn_2D_6 samples, was not saturated at magnetic field up to 5 T.

4. Conclusions

The novel intermetallic deuteride YMn_2D_6 was successfully synthesized under high deuterium pressure conditions. The structure of YMn_2D_6 (F-43m) differs dramatically from C15 symmetry (Fd-3m) of the parent material. Such a great rearrangement of the metal lattice due to deuterium absorption is rather exceptional for C15 Laves phases. Some chemical and physical properties of YMn_2D_6 were also examined by several analytic methods. X-ray absorption spectroscopy indicates progressive filling of the Mn d-band by electrons derived from deuterium which, in ionic form, occupies sites in the metallic lattice. During reaction

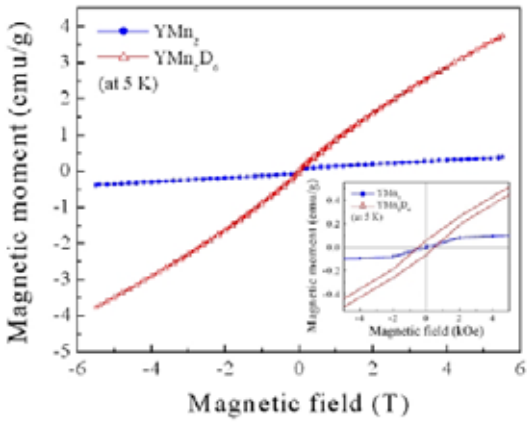

Fig. 7. Magnetization loops of YMn_2 and YMn_2D_6 measured at 5 K (H = −5 to 5 T).

of deuterium with YMn_2, leading to formation of YMn_2D_6, the changes of electronic structure, crystal symmetry, atomic environment and interatomic distances occur. Therefore the interpretation of magnetic properties of YMn_2D_6, which depend on so many factors, necessitates further measurements of low temperature specific heat, neutron diffraction, NMR, etc. These experiments are actually realized and new results will be published.

Acknowledgements

This research has been supported by the National Science Council of the Republic of China under the grant numbers NSC 92-2113-M-002-018 and NSC 92-2112-M-110-017.

References

[1] A.E. Dwight, Trans. Am. Soc. Met. 53 (1961) 479.
[2] H. Yamada, M. Shimizu, Phys. Lett. A 117 (1986) 313.
[3] Y. Nakamura, M. Shiga, S. Kawano, Physica B 120 (1983) 212.
[4] H. Wada, H. Nakamura, K. Yoshimura, M. Shiga, Y. Nakamura, J. Magn. Magn. Mater. 70 (1987) 134.
[5] T. Okamoto, H. Nagata, H. Fujii, Y. Makihara, J. Magn. Magn. Mater. 70 (1987) 139.
[6] M. Shiga, H. Wada, H. Nakamura, K. Yoshimura, Y. Nakamura, J. Phys. F 17 (1987) 1781.
[7] G. Oomi, T. Terada, M. Shiga, Y. Nakamura, J. Magn. Magn. Mater. 70 (1987) 137.
[8] R. Ballou, J. Deportes, R. Lemaire, Y. Nakamura, B. Ouladdiaf, J. Magn. Magn. Mater. 70 (1987) 129.
[9] K. Yoshimura, Y. Nakamura, J. Magn. Magn. Mater. 40 (1983) 55.
[10] H. Nakamura, N. Metoki, S. Suzuki, F. Takayanagi, M. Shiga, J. Phys.: Condens. Matter 13 (2001) 475.
[11] S. Asano, S. Ishida, J. Magn. Magn. Mater. 70 (1987) 39.
[12] H. Yamada, M. Shimizu, J. Magn. Magn. Mater. 70 (1987) 47.
[13] H. Fuji, M. Saga, T. Okamoto, J. Less-Common Met. 130 (1987) 25.
[14] J. Przewoznik, V. Paul-Boncour, M. Latroche, A. Percheron-Guegan, J. Alloys Compd. 225 (1995) 436.
[15] M. Latroche, V. Paul-Boncour, J. Przewoznik, A. Percheron-Guegan, F. Bouree-Vigneron, J. Alloys Compd. 231 (1995) 99.
[16] M. Latroche, V. Paul-Boncour, A. Percheron-Guegan, F. Bouree-Vigneron, J. Alloys Compd. 274 (1998) 59.
[17] H. Figiel, A. Lindbaum, Cs. Kapusta, E. Gratz, J. Alloys Compd. 217 (1995) 157.
[18] H. Figiel, J. Przewoznik, V. Paul-Boncour, A. Lindbaum, E. Gratz, M. Latroche, M. Escorne, A. Percheron-Guégan, P. Mietniowski, J. Alloys Compd. 274 (1998) 29.
[19] H. Fujii, M. Saga, T. Okamoto, J. Less-Common Met. 130 (1987) 25.
[20] I.N. Goncharenko, I. Mirebeau, A.V. Irodova, E. Suard, Phys. Rev. B 56 (1997) 2580.
[21] M. Latroche, V. Paul-Boncour, A. Percheron-Guégan, F. Bourée-Vigneron, G. André, Physica B 276 (2000) 666.
[22] M. Latroche, V. Paul-Boncour, A. Percheron-Guégan, F. Bourée-Vigneron, G. Andre, Physica B 234 (1997) 599.
[23] J. Przewoznik, J. Zukrowski, K. Krop, J. Magn. Magn. Mater. 140 (1995) 807.
[24] S.M. Filipek, V. Paul-Boncour, A. Percheron-Guegan, I. Jacob, I. Marchuk, M. Dorogova, T. Hirata, Z. Kaszkur, J. Phys.: Condens. Matter 13 (2001) 475.
[25] M. Latroche, V. Paul-Boncour, A. Percheron-Guégan, F. Bourée-Vigneron, G. André, J. Solid State Chem. 154 (2000) 398.
[26] B. Baranowski, S.M. Filipek, High pressure chemical synthesis, J. Jurczak, B. Baranowski, editors, Elsevier, Amsterdam, pp. 55–100.
[27] D. Fruchart, A. Rouault, C.B. Shoemaker, D.P. Shoemaker, J. Less-Common Met. 73 (1980) 363.
[28] A.V. Irodova, O.A. Lavrova, G.V. Laskova, L.N. Padurets, Sov. Phys. Solid State 24 (1982) 22.
[29] V. Paul-Boncour, A.P. Guégan, J. Alloys Compd. 293–295 (1999) 237.
[30] S. Matar, V. Paul-Boncour, Proceedings of the groupement francais de spectroscopie mössbauer, Juins, Bordeaux, 1998.

ARTICLE IN PRESS

Available online at www.sciencedirect.com

SCIENCE DIRECT®

Journal of Solid State Chemistry 178 (2005) 356–362

JOURNAL OF SOLID STATE CHEMISTRY

www.elsevier.com/locate/jssc

Neutron diffraction study, magnetic properties and thermal stability of YMn_2D_6 synthesized under high deuterium pressure

V. Paul-Boncour[a,*], S.M. Filipek[b], M. Dorogova[b], F. Bourée[c], G. André[c], I. Marchuck[b], A. Percheron-Guégan[a], R.S. Liu[d]

[a]*Laboratoire de Chimie Métallurgique des Terres Rares, CNRS, 2-8 rue Henri Dunant, 94320 Thiais Cedex, France*
[b]*Institute of Polish Chemistry. PAN, UL. Kasprzaka 44/52, 01224 Warsaw, Poland*
[c]*Laboratoire Léon Brillouin,CEA-CNRS, CEA/Saclay, 91191 Gif-sur-Yvette, France*
[d]*Department of Chemistry, National Taiwan University, Taipei 106, Taiwan, ROC*

Received 23 April 2004; accepted 28 May 2004

Abstract

A new phase YMn_2D_6 was synthesized by submitting YMn_2 to 1.7 kbar deuterium pressure at 473 K. According to X-ray and neutron powder diffraction experiments, YMn_2D_6 crystallizes in the $Fm\bar{3}m$ space group with $a = 6.709(1)$ Å at 300 K. The Y and half of the Mn atoms occupy statistically the 8*c* site whereas the other Mn atoms are located in 4*a* site and surrounded by 6 D atoms (24 e). This corresponds to a K_2PtCl_6-type structure with a partially disordered substructure which can be written as $[YMn]MnH_6$. No ordered magnetic moment is observed in the NPD patterns and the magnetization measurements display a paramagnetic behavior. The study of the thermal stability by Differential Scanning Calorimetry and XRD experiments indicates that this phase decomposes in YD_2 and Mn at 625 K, and is more stable than $YMn_2H_{4.5}$.

Keywords: Laves phase; Hydride; High pressure; X-ray diffraction; Neutron diffraction; Magnetism; Differential thermal calorimetry; Thermal stability

1. Introduction

Treatment of metals and alloys by using high hydrogen/deuterium pressure proved to be effective in the syntheses of new hydrides or deuterides. It has been used for binary hydrides like NiH [1] and nickel alloys [2,3], MnH_x [4], FeH_x [5]. More details can be found in several monographs [6–8]. With few exceptions (MnH_x can be given as example) the hydrides formed at high hydrogen pressure are not stable at normal conditions. We expected that the application of high hydrogen pressure to RT_2 (R = rare-earth and T = transition metal intermetallic compounds) may extend the hydrogen absorption to higher values with formation of new crystalline phases remaining stable at normal conditions.

As expected, we succeeded to form and study new hydrides (deuterides) of Laves-phase compounds like $ZrCo_2H_2$ and $ZrFe_2H_{3.6}$ [9,10], YFe_2H_5 and $ErFe_2H_5$ [11,12] and more recently YMn_2H_6 [13]. The hydrogen content stored in YMn_2H_6 corresponds to a weight capacity of 3% which is the largest value for such compound and is comparable to what is obtained in ZrV_2H_6 for example [14].

The previous X-ray diffraction (XRD) analysis has shown that YMn_2H_6 crystallizes in a face-centered cubic structure ($a = 6.707$ Å) [13]. This structure is quite different from that observed for the already known YMn_2H_x hydrides (deuterides) ($0 < x \lesssim 4.5$) which retains a structure derived from the cubic $MgCu_2$ type structure of YMn_2. At room temperature these hydrides show an increase of the cubic cell parameter up to

*Corresponding author. Fax: +33 1 49 78 12 03.
E-mail address: paulbon@glvt-cnrs.fr (V. Paul-Boncour).

0022-4596/$ - see front matter © 2004 Elsevier Inc. All rights reserved.
doi:10.1016/j.jssc.2004.05.066

$x = 3.5$ and a rhombohedral distortion for $4 \leqslant x \leqslant 4.5$ [15–20]. In contrast to these rather small distortions it seems that the crystal structure of YMn_2H_6 results from a complete reorganization of the unit cell of the parent compound, but to check this assumption it is necessary to determine also the location of the H atoms. For this purpose we have investigated the crystal structure of YMn_2D_6 using neutron powder diffraction (NPD) experiments. The magnetic structure was also studied by the NPD analysis and magnetic measurements. In order to determine the thermal stability of YMn_2D_6 we used the Differential Scanning Calorimetry (DSC) measurements and sample characterization by XRD after various heat treatments. These results are presented in this paper and discussed in relation with the properties of the $YMn_2H_{4.5}$ hydride.

2. Experimental

YMn_2 was prepared by induction melting of the pure elements (Y, 99.9% from Santoku America and Mn 99.99% from alpha products) followed by an annealing treatment of 11 days at 1073 K. The homogeneity of the sample was checked by XRD and electron microprobe analysis (EPMA). The intermetallic sample was single phase with a cubic C15 structure and $a = 7.681(1)$ Å. About 6 g of YMn_2D_6 has been prepared for the neutron diffraction experiments under 1.7 kbar deuterium pressure and 473 K [13]. The $YMn_2H_{4.5}$ hydride was synthesized as in Ref. [20]. After deuteration the powder remains black and the sample is stable under air during several months.

Density measurements have been performed using a volumetric method with an Accupyc 1330 Picnometer from Micromeritics Company.

The XRD patterns were measured with a D8 Brucker diffractometer equipped with a rear graphite monochromator in the range $10° < 2\theta < 120°$ with a step of 0.02° using Cu$K\alpha$ radiation. The samples were deposited on a flat plate with 0.2 mm thickness.

The NPD patterns of the deuteride have been registered at 2 and 80 K on the 3T2 diffractometer and at 1.5, 80 and 290 K on the G4.1 diffractometer at the Laboratoire Léon Brillouin (LLB) at Saclay. For the 3T2 experiment the wavelength was 1.225 Å and the angular range $6° < 2\theta < 125°$ with a step of 0.05°. For the G4.1 experiments the wavelength was 2.427 Å and the angular range was $2° < 2\theta < 82°$ with a step of 0.1°. The deuteride sample was contained in a vanadium tube of 8 mm diameter. All the XRD and NPD patterns were refined with the Rietveld method, using the Fullprof code [21]. The line shapes were refined with a Pearson VII function.

DSC was performed on TA-Q100 DSC apparatus from TA Instrument. The samples were placed in aluminum pans under flowing purified argon atmosphere. The experiments were performed from 313 K up to temperatures ranging from 523 to 750 K with a rate of 20 K/min.

Magnetization measurements were performed from 5 to 290 K on a Quantum Design PPMS magnetometer with applied field up to 5 T.

3. Results and discussion

3.1. Structure

Density measurements led to a value of $d = 4.63(1)\,g/cm^3$. This experimental density is in good agreement with the calculated one: $d = 4.636\,g/cm^3$ for YMn_2D_6 in a fcc cell with $a = 6.709$ Å and $Z = 4$.

The G4.1 experiments performed at various temperatures, between 1.5 and 290 K, revealed very few changes in the NPD patterns: a small increase of the background as the temperature increases and a shift of the peaks due to the increase of the cell parameter.

To solve the nuclear structure we have analyzed the NPD pattern measured at 2 K on 3T2. In a previous work [13] the XRD pattern of YMn_2D_6 was refined in a cubic structure described in the $F\bar{4}3m$ space group where the Y is on the 4*a* site and the Mn on 4*b* and 4*c* sites. Using this space group description, a Fourier difference of the experimental and calculated NPD pattern indicated that the D atoms should occupy the 24 g position with x close to 0. Nevertheless this solution led to very bad refinement of the NPD pattern with an R_{Bragg} of 43%. The Fourier difference analysis revealed that no other sites were occupied but that the density was too large or too small on the 4*a* and 4*b* sites depending on whether it was occupied by Y or Mn atoms. A good refinement ($R_{Bragg} = 6.3\%$) was obtained with a statistical occupation of Y and Mn atoms in the 4*a* and 4*b* positions. This structure can be also described in the $Fm\bar{3}m$ space group (supergroup of $F\bar{4}3m$) corresponding to the crystal structure (K_2PtCl_6 type structure) of Mg_2FeH_6 [22] and other isostructural M_2TH_6, hydrides [23,24], where M and T represent two different metals. In Mg_2FeH_6 the Mg atoms occupy the 8*c* site, Fe the 4*a* site and D atoms the 24*e* site. But as determined previously, the NPD pattern could not be refined in an ordered structure (for example Mn on 8*c* and Y on 4*e* sites led to an R_{Bragg} of 120%). The only solution to refine correctly the NPD line intensities was to assume a statistical occupancy of the 8*c* site by 4 Y and 4 Mn (Mn1) atoms, whereas the 4*a* site is occupied by 4 other Mn (Mn2) atoms and the 24*e* site by the D atoms (Table 1). This crystal structure led also to a better refinement of the XRD pattern at 300 K ($R_{Bragg} = 5.81\%$) than in the ordered structure described in the $F\bar{4}3m$ space group ($R_{Bragg} = 8\%$) [13].

Table 1
Unit cell parameter (a), cell volume (V), wave length (λ), refined atomic positions (x), occupation numbers (N), Debye–Waller factor (B), line width parameters (U, V, W, Y) and reliability factors (R_I,R_{wp},R_{exp},χ^2) for YMn_2D_6 NPD pattern measured on 3T2 at 2 K. Total number of independent reflections: 48

Space group	$Fm\bar{3}m$	$a = 6.6894$ (1) Å	$V = 299.34$ (1) Å^3	$\lambda = 1.225$ Å
Atoms	Wyckoff position	x	N	B (Å^2)
Y	8c		0.49(1)	0.09(4)
Mn1	8c		0.51(1)	0.00(4)
Mn2	4a		1	0.00(4)
D	24e	0.2465(3)	1	1.50(2)
$U = 1.48(2)$	$V = -0.50$	$W = 0.25$	$Y = 0.12(1)$	
$R_{Bragg} = 7.1\%$		$R_{wp} = 5.0\%$		
$R_{exp} = 2.2\%$		$\chi^2 = 5.1$		

Weak additional lines due to few percent (5.8%) of rhombohedral deuteride $YMn_2H_{4.5}$ and Y_2O_3 (2.5%) were observed in the XRD pattern. Very small additional lines were also observed in the NPD pattern, but much weaker than in the XRD pattern since the neutron have a larger penetration length than the X-ray, and are therefore less sensitive to the surface. The 3T2 NPD (2 K) pattern refined as described in Table 1 is reported in Fig. 1. The refinement of the 3T2 NPD pattern at 80 K leads to the same structure as that at 2 K with only a small increase of the cell parameter ($a = 6.6894(1)$ Å at 2 K and $a = 6.6909(1)$ Å at 80 K). The NPD patterns of YMn_2D_6 measured on G4.1 diffractometer (devoted to the study of magnetic structure) contains weak additional reflections at low angles, which cannot be refined in the fcc cubic cell of YMn_2D_6. However, all of them can be refined with the nuclear (3%) and magnetic structure of rhombohedral $YMn_2D_{4.5}$ (Fig. 2) [16,25].

Fig. 3 shows a schematic representation of the cubic structure of YMn_2D_6 described in the $Fm\bar{3}m$ space group. The coordination numbers and the calculated interatomic distances of the first neighbors are reported in Table 2.

The random (Y, Mn) substitution on the 8c site is rather surprising if we consider the difference between the metallic atomic radius of Y (1.80 Å) and Mn (1.40 Å) atoms. However, this difference is reduced if instead of metallic radii the covalent radii are considered Y(1.62 Å) and Mn (1.39 Å). In addition the small bump observed around $d = 4.74$ Å in both 3T2 and G4.1 NPD patterns can indicate a short range order, which correspond to the distance between two Y(Mn1) or two Mn2 atoms. Since no short range order between two Mn2 atoms is expected, it can rather be related to the existence of a short range order of Y and Mn atoms on the 8c site.

Another important feature is that the deuterium atoms are not located into interstitial sites (A2B2 or AB3) like in other YMn_2H_x hydrides but form octahedra around the Mn2 atoms. The distances between the D atoms ($d = 2.34$ Å) are larger than the

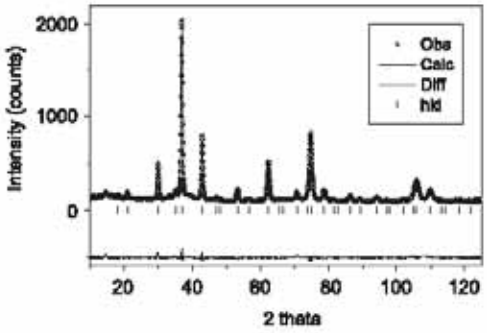

Fig. 1. Experimental and refined NPD pattern of YMn_2D_6 measured on 3T2 at 2 K.

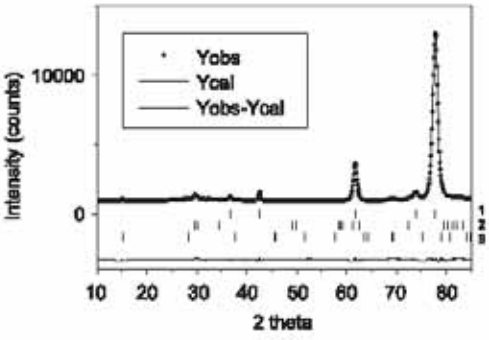

Fig. 2. NPD pattern of YMn_2D_6 measured on G41 at 1.5 K. The tick correspond to the (hkl) of (1) YMn_2D_6, (2) nuclear and (3) magnetic structure of $YMn_2D_{4.5}$.

Switendik criterium $d = 2.1$ Å [26], whereas the Mn2–D distances (1.65 Å) are shorter than the sum of the atomic metallic radius (1.75 Å). A comparison with $YMn_2D_{4.5}$ which crystallizes in the rhombohedral $R\bar{3}m$ space group with 2 Y sites, 2 Mn sites and 3 D sites [16,25] also indicates a change of bonding type. In $YMn_2D_{4.5}$ each

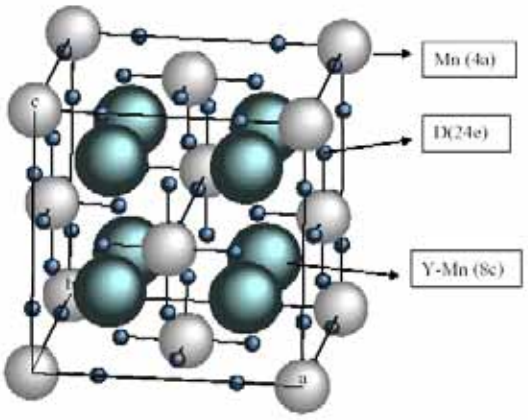

Fig. 3. Schema of the cubic structure of YMn_2D_6.

Table 2
Coordination numbers and interatomic distances in YMn_2D_6 calculated with $a = 6.709(1)$ Å measured at 300 K

Central atom	Y–Mn1 (Å)	Mn2 (Å)	D (Å)
Y–Mn1 (8*c*)	12–4.744(1)	4–2.905(1)	12–2.372(1)
Mn2 (4*a*)	8–2.905(1)	12–4.744(1)	6–1.654(7)
D (24*e*)	4–2.372(1)	1–1.654(7)	4–2.339(10)

Mn atom is surrounded by 6 Mn at 2.89–2.92 Å whereas in YMn_2D_6, taking into account the half occupancy of the 8*c* site, each Mn is surrounded by 4 Mn at 2.90 Å. This means that if the Mn–Mn interatomic distances are conserved, the Mn coordination numbers changes significantly. The distances between the Y and Mn atoms in $YMn_2D_{4.5}$ varies between 3.39 and 3.43 Å which is large compared to 2.905 Å in YMn_2D_6. This confirms a significant change in the nature of the bonding between Y and Mn atoms.

In $YMn_2D_{4.5}$ the Mn–D distances varies between 1.77 and 1.92 Å and the Y–D distance between 2.188 and 2.386 Å. These distances are larger than the Mn2–D distances (1.654 Å) observed in YMn_2D_6 and also suggest a different type of Mn–D bonding.

This raises the question if the magnetic order in YMn_2D_6. $YMn_2D_{4.5}$ is antiferromagnetic with a moment of 3.2 μB by Mn atoms at 1.5 K and a Néel temperature of 330 K [25]. The analysis of the NPD patterns of YMn_2D_6 from 1.5 to 290 K has revealed that there is no long-range ordered magnetic structure associated with this phase. The magnetization curves display a linear behavior down to 50 K and should be related to a paramagnetic behavior (Fig. 4). At 5 K there is a weak ferromagnetic component, which can be attributed to small amount of secondary phases or impurities. The inverse of the magnetic susceptibility is

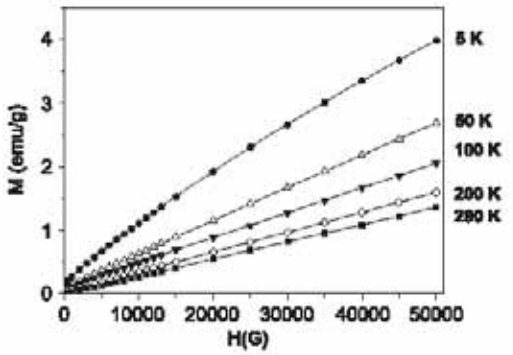

Fig. 4. Magnetization curves of YMn_2D_x at various temperatures.

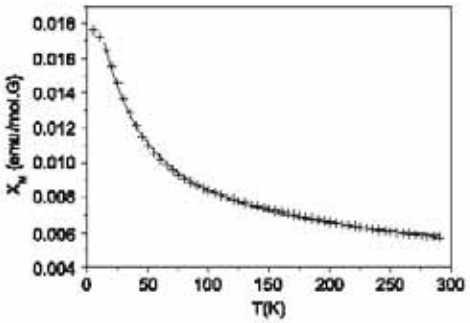

Fig. 5. Evolution of the molar susceptibility of YMn_2D_6 (+) and refinement (line) with a Pauli paramagnet constant susceptibility and a Curie–Weiss law.

not linear versus temperature indicating that this evolution is not related to a simple Curie–Weiss law. However, it is possible to refine (Fig. 5) the magnetic molar susceptibility χ_M with the sum of a Pauli paramagnet temperature independent susceptibility and a Curie–Weiss law:

$$\chi_M = \chi_0 + \frac{C}{T - \theta_p} \quad (1)$$

with $\chi_0 = 0.004 \pm 0.001$ emu/mol, $C = 0.55$ emu/mol K G and $\theta_p = -30$ K. Assuming that the Curie–Weiss law concerns half the Mn atoms this would lead to an effective Mn moment of about 3 μ_B close to that observed in other YMn_2 hydrides. Since the shorter Mn–Mn distances in YMn_2D_6 are similar to those of $YMn_2D_{4.5}$ (2.90 Å), one would have expected the existence of an ordered antiferromagnetic or ferrimagnetic structure for YMn_2D_6. However, due to the strong Mn2–D bonding, the interaction between the Mn1 and Mn2 atoms in YMn_2D_6 should be very different from that observed in $YMn_2D_{4.5}$. Goncharenko et al. [27] have shown that the Mn–Mn interactions in $RMn_2H_{4.5}$

hydrides are very sensitive to the hydrogen surrounding and could be either ferromagnetic or antiferromagnetic depending of the presence or absence of one H atom between the two Mn atoms. In the case of YMn_2D_6, the octahedral cage of deuterium atoms seems to prevent any long range order magnetic interaction.

3.2. Thermal stability

Fig. 6 displays the evolution of the DSC signal of $YMn_2H_{4.5}$ and YMn_2D_6 up to 673 K. In order to identify the origin of these peaks, XRD measurements were performed on $YMn_2H_{4.5}$ and YMn_2D_6 after different heating temperatures in the DSC apparatus as summarized in Table 3. The H content in the YMn_2H_x phases was estimated from their cell parameters using the data of Ref. [20].

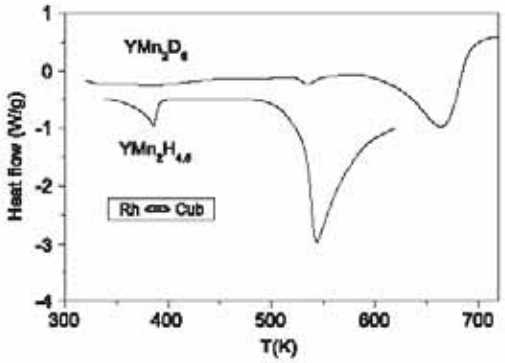

Fig. 6. Evolution of the DSC signal versus temperature for $YMn_2H_{4.5}$ and YMn_2D_6.

The endothermic peak observed for $YMn_2H_{4.5}$ at 386 K (41.57 J/g) can be attributed to the reversible rhombohedral–cubic transformation according to previous ND measurements [16]. A detailed DSC analysis, with temperature cycles at every 5 K, indicates that this peak intensity progressively decreases as the heating temperature is raised between 445 and 520 K due a loss of hydrogen in $YMn_2H_{4.5}$ until complete disappearance of the rhombohedral phase.

A second broad endothermic peak is observed around 540 K for $YMn_2H_{4.5}$, with a large enthalpy of reaction ($\Delta H = 190$ J/mol). According to the XRD analysis of $YMn_2H_{4.5}$ between 523 and 593 K this peak can be attributed to a fast deuterium desorption from $x = 3.5$ to 1.8 H/f.u. (Table 3). As temperature is higher, slower hydrogen desorption takes place. The XRD analysis indicates that after heating at 643 K there is a partial decomposition of the hydride into YH_2 and Mn, and probably a beginning of amorphization beside a remaining crystalline $YMn_2H_{0.1}$ phase.

Concerning YMn_2D_6, a very small peak is also observed at 386 K due to the 2–3% of rhombohedral

Table 3
XRD results for $YMn_2H_{4.5}$ and YMn_2D_6 after DSC experiments

T_{max} (K)	$YMn_2H_{4.5}$			YMn_2D_6		
	Phase	%	Cell parameter (Å)	Phase	%	Cell parameter (Å)
298	$YMn_2H_{4.5}$	100	$a = 5.860(1)$ $c = 14.07(2)$	YMn_2D_6 $YMn_2D_{4.5}$	93 7	$a = 6.709(1)$ $a = 5.860(1)$ $c = 14.07(2)$
493	$YMn_2H_{4.5}$	95	$a = 5.860(1)$ $c = 14.07(1)$			
	$YMn_2H_{3.7}$	5	$a = 8.138(1)$			
523	$YMn_2H_{3.5}$	34	$a = 8.113(1)$	YMn_2D_6	100	$a = 6.707(1)$
	$YMn_2H_{2.5}$	66	$a = 8.013(1)$			
573	$YMn_2H_{2.1}$	28	$a = 7.975(1)$	YMn_2D_6	100	$a = 6.705(1)$
	$YMn_2H_{1.9}$	72	$a = 7.952(1)$			
593	$YMn_2H_{1.6}$	100	$a = 7.922(1)$	YMn_2D_6 YD_2	62 38	$a = 6.705(1)$
623	$YMn_2H_{1.4}$	100	$a = 7.909(1)$	YMn_2D_6 YD_2 Mn	22 35 42	$a = 6.688(2)$ $a = 5.139(9)$ $a = 8.922(5)$
643	$YMn_2H_{0.1}$ YH_2 Mn	10 36 55	$a = 7.727(1)$ $a = 5.147(1)$ $a = 8.890(4)$			
673	YH_2 Mn			YD_2 Mn	44 55	$a = 5.139(9)$ $a = 8.922(5)$

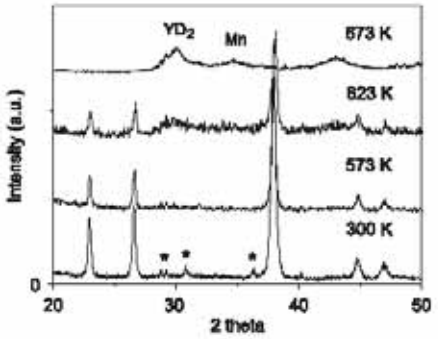

Fig. 7. Evolution of the YMn_2D_6 patterns after various DSC treatments. The temperatures correspond to the DSC experiment maximum temperatures. The stars are related to second phase: rhombohedral and cubic deuteride.

$YMn_2D_{4.5}$. The peak at 540 K can also be attributed to the desorption of the remaining YMn_2D_x phases since this intensity (6 ± 1 J/g) represents only 3% of that observed for $YMn_2H_{4.5}$. This is confirmed by the fact that the lines attributed to $YMn_2D_{4.5}$ have disappeared from the XRD pattern of YMn_2D_6 after heating at 573 K (Fig. 7). The large endothermic peak observed for YMn_2D_6, which starts at 611 ± 2 K with a maximum at 664 ± 2 K and an enthalpy of 200 ± 2 J/g can be attributed to the deuteride decomposition into YD_2 and α-Mn which is complete at 673 K (Fig. 7). The relative percentage of YD_2 and Mn correspond to a full decomposition and should be accompanied by a desorption of about 4 H/f.u. A weak decrease of the cubic cell parameter of YMn_2D_6 (−0.3%) was observed when increasing the temperature (Table 3) which may imply a very small deuterium desorption.

These results clearly show that YMn_2D_6 displays a larger stability than $YMn_2H_{4.5}$ since its thermal decomposition occurs at higher temperature. The origin of this higher stability can be explained by the fact that the Mn–D bonds are stronger in YMn_2D_6 than in $YMn_2H_{4.5}$. In YMn_2D_6 the Mn–D bonds have a length of 1.65 Å, whereas they are equal or larger than 1.78 Å in $YMn_2H_{4.5}$. In addition in $YMn_2H_{4.5}$ the H atoms are located in interstitial A2B2 tetrahedral sites and H desorption results in the formation of hydrides with lower H content in the same type of structure. In YMn_2D_6 there is a complete reorganization of the metallic framework which is different from that of the starting compound YMn_2 and therefore the simple hydrogen or deuterium desorption is not possible.

3.3. Discussion

This study has shown that YMn_2D_6 synthesized by submitting YMn_2 to very high hydrogen pressure (1.7 kbar) display a fluorite-type structure with a disordered substructure. Several isostructural hydrides of M_2TH_6 where M is a alkaline earth (M = Mg, Ca, Sr) or a divalent rare earth metal (M = Eu,Yb) and T a transition metal (T = Fe, Ru, Os) have already been obtained by sintering the mixture of metallic powder at moderate temperatures (623–800 K) and hydrogen pressure of 70–130 bars [24]. In these compounds the parent intermetallic compounds does not exist and direct hydrogenation is not possible [24].

However, it is the first time to our knowledge that this type of hydride can be obtained by direct reaction of an intermetallic compound with hydrogen (deuterium). Moreover in YMn_2D_6 the 8*c* site is not a divalent metal but a result from a random distribution of Y and Mn atoms. This marks also a difference with the quaternary complex hydrides $M_1M_2TH_6$ (M_1M_2 = CaMg and T = Fe) where an ordered arrangement of the alkaline metal on the 8*c* site was found [24].

Concerning the nature of the Mn–D bonds it can be noticed that the Mn2–D distances (d(Mn–D) = 1.65 Å) are close to those observed in other M_2TH_6 hydrides [24]. For example, in Mg_2FeH_6, d(Fe–D) = 1.556 Å and in Mg_2OsH_6, d(Os–D) = 1.682 Å. These short distances are indicative of covalent bonding [22]. These hydrides can therefore be considered as coordination compounds rather than interstitial metal hydrides. In addition these M_2TH_6 compounds are described as complex anions TH_6^{4-} surrounded by a cage of divalent M^{2+} cations. Assuming the same type of electronic configuration and applying the 18 electrons rule the Mn2–D should form $[Mn^{I}D_6]^{5-}$ octahedral complex [28] whereas the Mn1 on the 8*c* site should be Mn^{II}, if we consider that the Y atoms are Y^{III}. However the ionic state of the Mn atoms is not supported by the previous X-ray absorption (XAS) measurements on YMn_2D_6 which have shown that the Mn L_{2-3} near edge structure are similar to that of Mn in YMn_2 [13]. The Mn *K*-edge near edge structure is also close to that observed for $YMn_2H_{4.5}$. Compared to the starting intermetallic YMn_2 there is a decrease of the prepeak intensity corresponding to a transition from 1*s* state to empty 4*p* states hybridized with the 3*d* conduction band. This prepeak intensity progressively decrease as the H content increases as observed in other RM_2H_x hydrides [29]. These XAS results indicate that the Mn atoms are not in an ionic state since this would induce a significant shift of the Mn *K*-edge position compared to YMn_2 and the other YMn_2H_x related hydrides. Nevertheless the analysis of the magnetic susceptibility with the sum of a Pauli paramagnet and a Curie–Weiss paramagnet, may indicate different magnetic behavior for the Mn1 and Mn2 atoms, in relation with their very different surrounding. Therefore, band structure calculations will be performed in order to get a better understanding of the electronic structure of YMn_2D_6. In addition Nuclear Magnetic Resonance of

^{55}Mn is in progress to clarify the nature of the two types of Mn atoms in this new deuteride.

4. Conclusion

In this study, we have shown that YMn_2D_6 crystallizes in a disordered fluorite structure which is close to other hydrides like Mg_2FeH_6 and can be denoted as $[YMn]MnH_6$. The Mn atoms occupy two types of sites: half of them are randomly substituted with the Y atoms on the 8*c* site while the other occupy the 4*c* site and are surrounded by 6 deuterium atom at 1.65 Å. The neutron experiments down to 1.5 K did not reveal any ordered magnetic structure for this compound. The magnetic curves were analyzed assuming a sum of Pauli and Curie–Weiss paramagnetic behavior resulting from two different types of Mn atoms, due to their very different D surrounding. The study of the thermal decomposition of YMn_2D_6 and $YMn_2H_{4.5}$ hydrides though DSC and XRD experiments indicate a higher thermal stability for YMn_2D_6. This can be attributed to the stronger Mn–D bonding and the difference in the structure compared to the C15 one of the parent compound.

Acknowledgments

We are thankful to V. Lalanne for the synthesis of YMn_2 and E. Leroy for the EPMA analysis.

References

[1] B. Baranowski, R. Wisniewski, Bull. Acad. Pol. Sci. 14 (1966) 273.
[2] S.M. Filipek, B. Baranowski, Rocz. Chem. 49 (1975) 1149.
[3] S.M. Filipek, B. Baranowski, M. Yoneda, Rocz. Chem. 51 (1977) 2243.
[4] M. Krukowski, B. Baranowski, Rocz. Chem. 49 (1975) 1183.
[5] V.E. Antonov, I.T. Belash, E.G. Ponyatovskii, Scr. Metall. 16 (1982) 203.
[6] E.G. Ponyatovskii, V.E. Antonov, I.T. Belash, in: A.M. Prokhorov, A.S. Prokhorov (Eds.), Problems in Solid State Physics, Mir Publ., Moscow, 1984, pp. 109–171.
[7] B. Baranowski, S.M. Filipek, in: B. Baranowski, J.J. Jurczak (Eds.), High Pressure Chemical Synthesis, Elsevier Science Publishers, Amsterdam, Oxford, New York, Tokyo, 1989.
[8] Y. Fukai, in: Y. Fukai (Ed.), The Metal–Hydrogen System, Basic Bulk Properties, vol. 21, Springer, Berlin, 1993, pp. 71–119.
[9] S.M. Filipek, I. Jacob, V. Paul-Boncour, A. Percheron-Guégan, I. Marchuck, D. Mogilyanski, J. Pielaszek, Pol. J. Chem. 75 (2001) 1921–1926.
[10] V. Paul-Boncour, F. Bourée, S.M. Filipek, I. Marchuck, I. Jacob, A. Percheron-Guegan, J. Alloys Compd. 356–357 (2003) 69–72.
[11] V. Paul-Boncour, S.M. Filipek, A. Percheron-Guégan, I. Marchuk, J. Pielaszek, J. Alloys Compd. 317–318 (2001) 83–87.
[12] V. Paul-Boncour, S.M. Filipek, I. Marchuck, G. André, F. Bourée, G. Wiesinger, A. Percheron-Guegan, J. Phys. 15 (2003) 4349–4359.
[13] C.-Y. Wang, V. Paul-Boncour, R.-S. Liu, A. Percheron-Guégan, M. Dorogova, I. Marchuck, T. Hirata, S.M. Filipek, H.-S. Sheu, L.-Y. Jang, J.-M. Chen, H.-D. Yang, Solid State Commun. 130 (2004) 815–820.
[14] J.-J. Didisheim, K. Yvon, G. Fischer, D. Shaltiel, J. Less-Common Met. 73 (1980) 355–362.
[15] M. Latroche, V. Paul-Boncour, J. Przewoznik, A. Percheron-Guégan, F. Bourée-Vigneron, J. Alloys Compd. 231 (1995) 99–103.
[16] M. Latroche, V. Paul-Boncour, A. Percheron-Guégan, F. Bourée-Vigneron, J. Alloys Compd. 274 (1998) 59–64.
[17] M. Latroche, V. Paul-Boncour, A. Percheron-Guégan, F. Bourée-Vigneron, G. André, Physica B 276–278 (2000) 666–667.
[18] H. Figiel, A. Lindbaum, C. Kapusta, E. Gratz, J. Alloys Compd. 217 (1995) 157–160.
[19] V. Paul-Boncour, M. Latroche, A. Percheron-Guégan, J. Solid State Chem. 150 (2000) 183–187.
[20] J. Przewoznik, V. Paul-Boncour, M. Latroche, A. Percheron-Guégan, J. Alloys Compd. 225 (1995) 436–439.
[21] J. Rodríguez-Carvajal, in: Proceedings of Congr. Int. Union of Crystallography, 1990, p. 127.
[22] J.-J. Didisheim, P. Zolliker, K. Yvon, P. Fischer, J. Schefer, M. Gubelmann, A.F. Williams, Inorg. Chem. 23 (1984) 1953–1957.
[23] E. Orgaz, M. Gupta, J. Phys. 5 (1993) 6697–6718.
[24] B. Huang, F. Bonhomme, P. Selvam, K. Yvon, P. Fischer, J. Less-Common Met. 171 (1991) 301–311.
[25] I.N. Goncharenko, I. Mirebeau, A.V. Irodova, E. Suard, Phys. Rev. B 56 (1997) 2580–2584.
[26] A.E. Switendick, Z. Phys. Chem. N. F. 117 (1979) 89.
[27] I.N. Goncharenko, I. Mirebeau, A.V. Irodova, E. Suard, Phys. Rev. B 59 (1999) 9324–9331.
[28] H. Kohlmann, Encyclopedia of Physical Science and Technology, Academic Press, New York, 2002, pp. 441–458.
[29] V. Paul-Boncour, A. Percheron-Guegan, J. Alloys Compd. 293–295 (1999) 237–242.